Onboard Payload Mass Estimation and Electric Propulsion Modeling for Multicopters with Application in Unmanned Aerial Systems

by

ABEL MARTINEZ MARTINEZ

Presented to the Faculty of the Graduate School of
The University of Texas at Arlington in Partial Fulfillment
of the Requirements
for the Degree of

MASTER OF SCIENCE IN AEROSPACE ENGINEERING

THE UNIVERSITY OF TEXAS AT ARLINGTON

May 2019

To my mother Josefa, my father Ginés, my sister Paloma and my grandmother Encarna.

ACKNOWLEDGEMENTS

I would like to express my deep and sincere gratitude to my research supervisor, Dr. Kamesh Subbarao for letting me be a part of the Aerospace System Laboratory and providing invaluable guidance throughout this research. Thank you for your help and for this opportunity. I would also like to thank Dr. Dudley Smith and Dr. Bernd Chudoba for their excellent courses and aeronautic vocation, thank you for your inspiration and motivation. I express my special thanks to Dr. Raúl Fenández, for being a member of my committee, a friend and an example to follow.

I would like to thank my colleagues at the Aerospace Systems Laboratory, Rajnish Bhusal, Diganta Bhattacharjee, Barış Taner, Katyayani Balachandran for their constant help, advice and guidance. Thank you for suffering the terrible noise of my experiments without complains. I am extending my thanks to Ameya Godbole for his cooperation in this thesis, helping me with ROS.

Special mention to my friends. Juan Diego Pelegrín Garcia and Pablo Bernal Alcázar, If I am here today, it is because I took you as mentors and examples of success. Paula Rivera Nicolás and Rafael Caulín Atienzar, we will never forget the American experience that we had together.

I owe all the good things in my life to my parents, my sister and my family. I thank them for all the sacrifices they have made to make my life happier. Thank you for providing me with the education and resources to achieve my dreams.

Finally, my thanks go to all the people who have supported me to complete the research work directly or indirectly.

May 9, 2019

ABSTRACT

Onboard Payload Mass Estimation and Electric Propulsion Modeling for Multicopters with Application in Unmanned Aerial Systems

ABEL MARTINEZ MARTINEZ, M.S

The University of Texas at Arlington, 2019

Supervising Professor: Kamesh Subbarao

Unmanned vehicles are the future. The aim of the future online retailers, delivery and transportation companies would be air delivery using unmanned aerial vehicles. Multicopters are becoming rapidly famous because they offer a relatively easy-to-fly platform that is also very stable, and their mechanical simplicity. The possibility of estimating the weight of the multicopter in real time is really useful. A weight estimation system that could be implemented in multicopters with cable suspended payloads without using any extra sensors is presented in this thesis.

The weight estimation system uses a functional relationship that correlates Pulse Position Modulation (PPM) signal and the battery voltage with the thrust produced. Monitoring PPM signal and the battery voltage the total thrust produced is estimated. Total weight is equal to total thrust when the multicopter is flying in hover.

Thrust, current drawn, power consumption, efficiency and RPM of the motors are also a function of PPM signal and the battery voltage. The estimation system was enhanced, extending its capability to estimate these performance parameters. A test bench was designed and built to conduct different experiments. As a result of

these experiments and further data processing functional relationship that correlates PPM signal and the battery voltage with thrust, current drawn, power consumption, efficiency and RPM was obtained. The estimation system was tested and validated. Finally, the test bench was used to test different ESC-Motors-Propeller combinations and compare their performance in terms of thrust, current drawn, power consumption, efficiency, RPM and motor temperature.

TABLE OF CONTENTS

LIST OF ILLUSTRATIONS

LIST OF TABLES

CHAPTER 1

INTRODUCTION

1.1 Background and Motivation

In recent years, electronics have experienced a drastic increase in computation power and reduction in size and cost. All these factors have propitiated the proliferation of the unmanned vehicles also known as "drones" and the emergence of new types of aircraft. The word "drone" includes all unmanned vehicles. But very often people use this word referring to multicopters. These aircraft are becoming rapidly famous because they offer a relatively easy-to-fly platform that is also very stable. Moreover, they are mechanically simpler and cheaper to build than other rotor-craft, for example helicopters.

Figure 1.1: DJI Mavic 2 Pro Quadcopter (Image Courtesy: store.dji.com)

Figure 1.2: DJI F550 Hexacopter (Image Courtesy: store.dji.com)

The most popular multicopters are quadcopters. A standard quadcopter has four symmetrically placed propellers with fixed pitch that are arranged in counter-rotating pairs, in "+", "h", or "x" configuration being the last one the most popular.

Hexacopters and octacopters are also popular. By increasing the number of rotors, stability is also increased, however, complexity will increase as well.

At one time, aerial unmanned vehicles used to be operated just for military purposes. But nowadays the use of these vehicles for civilian applications is spreading rapidly. Multicopters already have extensive uses: remote sensing [1], commercial aerial surveillance [2], commercial and motion picture film making [3], disaster relief [4], package delivery [5], rescue [6] and recreational uses are only a few examples. Companies have realized that unmanned vehicles are the future. The aim of the present and future online retailers, transportation and delivery companies would be air delivery using unmanned aerial vehicles [7]. There are personal transportation multicopter prototypes already under development [8], and we are not far from being witnesses of the personal aerial transportation revolution. This is an emergent field and future research will be focused in making multicopters fly better, faster, further, and safer. In the future, more and more aerospace companies will be dedicated to the development, production and maintenance of that kind aircraft.

The possibility of estimating the weight of the multicopter in real time is really useful. Specially for drones that are used to carry payload. This capability would make the multicopter able to estimate the payload weight as well. Using this feature, an air delivery vehicle could know if the payload is too heavy, or if there is sufficient battery to accomplish a mission.

There are already different approaches to determine a multirotor weight. In [9], a way to estimate the payload of a quadcopter with a grasper was derived. The authors estimated the change in the mass of the quadcopter when the grasper was used the grasper to carry objects. This change is estimated based on the dynamic equations of the force-linear acceleration and the torque-angular acceleration relations of the quadcopter. The measurements are taken as the quadcopter is perturbed

slightly around its hovering position. Recursive least squares estimation is then used to detect the payload change.

An alternative to the approach in [9] is to use an enhanced model of the quadcopter. In [10], a drag-force enhanced model is derived. The drag force is created from the interaction of the propeller with the air stream. Fundamental blade element theory is used to derive the entire dynamic model of a quadcopter. However, the experimental validation of the model is only done for the force model defining the relations between the rotation angles and the translational velocities. Two controllers based on the drag-force enhanced model are proposed. The resulting hardware implementations are only evaluated qualitatively by pointing out that the systems are much easier to fly with these new controllers.

The works of [10] is extended in [11]. An observer is presented and the mass estimation problem is approached from a different viewpoint: improving the translational velocity and attitude estimates using Inertial Measurement Unit (IMU) measurements. The improvement is due to a better dynamic model that correctly explains the physics related to the measured acceleration. In principle, it is shown that the accelerometers directly measure the translational velocity. However, the model parameters are based on the estimated values of the payload as well as the drag coefficient which are typically obtained using least squares optimization. In order to achieve consistent estimates, this method requires accurate measurements of the signals from a VICON (Indoor Motion Capture)system [12]. Consequently, this approach is usually not applicable when the quadcopter is operating outdoors. That makes impossible the implementation of the system in aerial delivery vehicles.

In [13], a different estimator is designed to detect the change of the mass of the quadcopter. The system takes the sensor behavior into consideration and only uses the measurements from the IMU and pilot commands to identify the useful

parameters. Hence, this approach could be applicable for small quadcopters where number of sensors is restricted. The dynamic models of the quadcopter are presented focused on the relation between the roll rate and lateral acceleration.

However, besides all the above limitations all of these mass estimation approaches have common problem. The payload has to be rigidly attached to the multicopter. This makes impossible the implementation of any of them in for example, multicopters with cable suspended payloads.

In the case of aerial delivery multicopters, the use of a cable to lift the payload could be really convenient. This allows the vehicle to pick up the payload without the need of landing. That results in a faster pick up process without the danger of rotating blades close to the people or the risk of crashing during the take off or landing. Avoiding an unnecessary take off and landing also increases efficiency.

This results in a new research field of developing a weight estimation system that could be implemented in multicopters with cable suspended payloads. In [14]a method to obtain individual motor thrust measurements is presented. The authors integrated strain gauges into the quadcopter frame to provide total force measurements on each arm of the vehicle. This method could be used for payload weight estimation and be implemented in multicopters with cable suspended payloads. However, it would add extra sensors to the vehicle. This would result in extra weight and complexity.

The ideal weight estimation system would not use extra sensors. Moreover, apart from weight estimation, the possibility of estimating thrust, current drawn, power consumption, efficiency and RPM in real time would be really interesting.

1.2 Problem Description

The primary goal of this thesis is to create a mass estimation system without any external sensor that would add weight, power consumption or complexity to the

multicopter design. This estimation system has to be able to be implemented in multicopters with cable suspended payloads. The secondary objective is to enhance this estimation system, extending its capability to estimate other performance parameters.

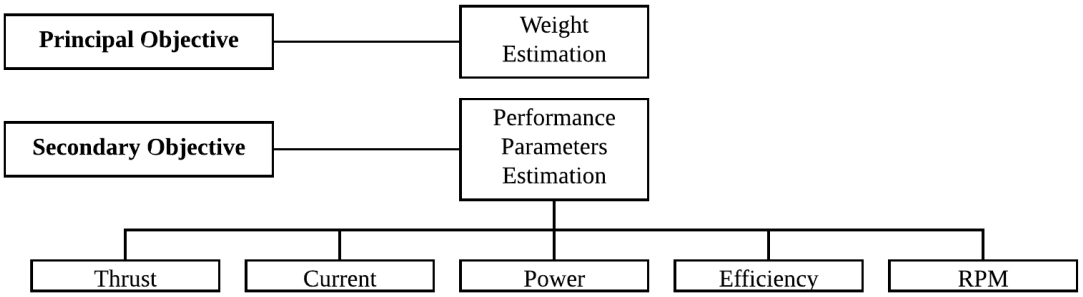

Figure 1.3: Principal and secondary objectives

Multicopters most commonly use brushless DC electric motors, driven by an electronic speed controller (ESC). These devices are controlled by Pulse Position Modulation (PPM) signal that comes from the flight controller.

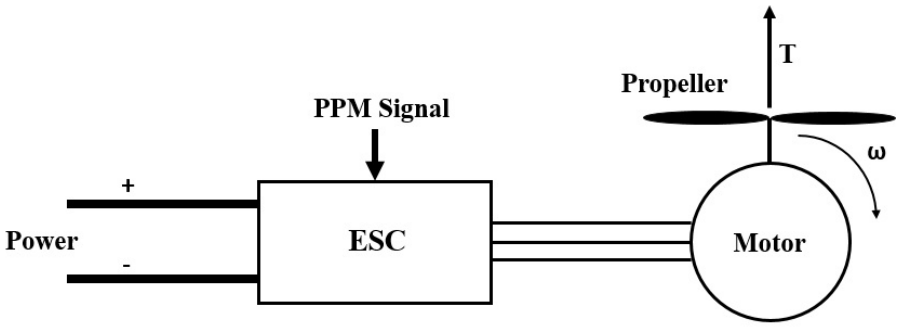

Figure 1.4: ESC-Motor

Performance parameters as thrust, current, power, efficiency and RPM for ESC-Motor-Propeller combination are a function of two variables:

- The PPM signal (x) sent to the motor´s ESC
- The voltage of the battery (v)

So thrust(T), current(I), power(P), efficiency (E) and RPM (R) can be expressed as:

$$\begin{aligned} T &= f_1(x, v) \\ I &= f_2(x, v) \\ P &= f_3(x, v) \\ E &= f_4(x, v) \\ R &= f_5(x, v) \end{aligned} \tag{1.1}$$

To obtain the functional relationship, several experiments were conducted to relate the voltage and PPM signal with thrust, current, power, efficiency and RPM.

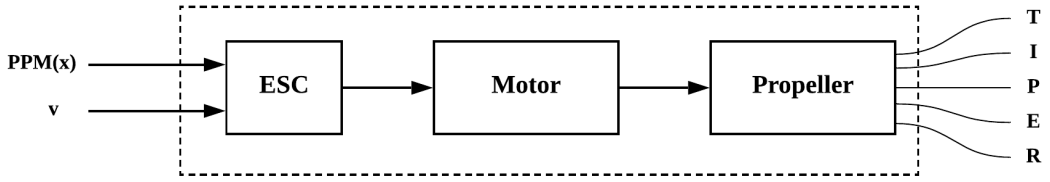

Figure 1.5: Functional relationship scheme

CHAPTER 2

WEIGHT ESTIMATION METHODOLOGY

In this chapter the methodology followed to achieve weight estimation is explained. The weight estimation system works using a functional relationship that correlates PPM signal x and the battery voltage v with the thrust produced T. This functional relationship has to be previously obtained experimentally. This functional relationship is specific for a ESC-Motor-Propeller combination, and is not valid if any of the three components is changed. Different functional relationships could be obtained in order to keep using the weight estimator if for example, the propellers were replaced by a different model. Furthermore, PPM signal x and battery voltage v need to be monitored.

The forces acting on a hovering multicopter with cable suspended payload are shown in figure 2.1:

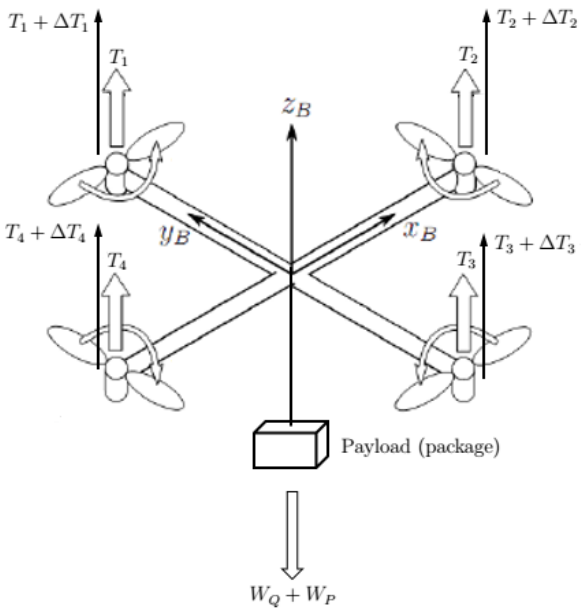

Figure 2.1: Quadcopter free body diagram

For a multicopter of n motors hovering, thrust and weight forces are in equilibrium:

$$T_1 + T_2 + T_3 + T_4 + ... + T_n = W_Q \tag{2.1}$$

where T_1, T_1, T_1, T_1,..., T_n are propeller thrust forces when there is no payload for the multicopter to hover, W_Q is the weight of the multicopter.

To calculate W_Q the multicopter has to be flown to hover at a height 'H' ft. The battery voltage v and the PPM signal of the n motors are recorded. Then using the functional representation the propeller thrust force for each propeller is obtain. Add all the n forces to get W_Q using equation 2.1.

If an external payload is attached and the multicopter is in hover:

$$T_1 + \Delta T_1 + T_2 + \Delta T_2 + T_3 + \Delta T_3 + T_4 + \Delta T_4 + ... + T_n + \Delta T_n = W_Q + W_P \quad (2.2)$$

where ΔT_1, ΔT_2, ΔT_3, ΔT_4,..., ΔT_n are additional propeller thrust forces needed to make the multicopter hover with the payload attached, and W_P is the weight of the payload.

Subtracting equation 2.1 from equation 2.2 the weight of the payload is obtained:

$$\Delta T_1 + \Delta T_2 + \Delta T_3 + \Delta T_4 + ... + \Delta T_n = W_P \quad (2.3)$$

CHAPTER 3

TEST BENCH DESIGN

A test bench was necessary to perform the experiments at the Aerospace Systems Laboratory (ASL). This empirical process finally would result in the ESC-Motor-Propeller functional relationship that correlates PPM signal x and the battery voltage v with T, I, P, E and R. As a part of this thesis, a test bench had to be designed and built. In [15], [16] and [17] another test benches where developed by other researchers for different porpuses. The test bench consists of an Arduino [18] type micro-controller and a set of sensors as shown in figure 3.1 measuring different parameters:

- Time in seconds
- PPM signal in μs
- Thrust in grams
- Voltage in volts
- Current in amps
- Power in watts
- Efficincy in g/watt
- RPM
- Room temperature in ^{o}C
- Motor temperature in ^{o}C

The data acquisition process was automated by interfacing the test bench with MATLAB [19]. The computer receives and stores the information sent by the micro-controller during the experiments. The results are structured in packages and stored

in MATLAB files for further analysis. The test bench is connected to a computer via USB cable. The micro-controller is communicating with MATLAB via Serial Port.

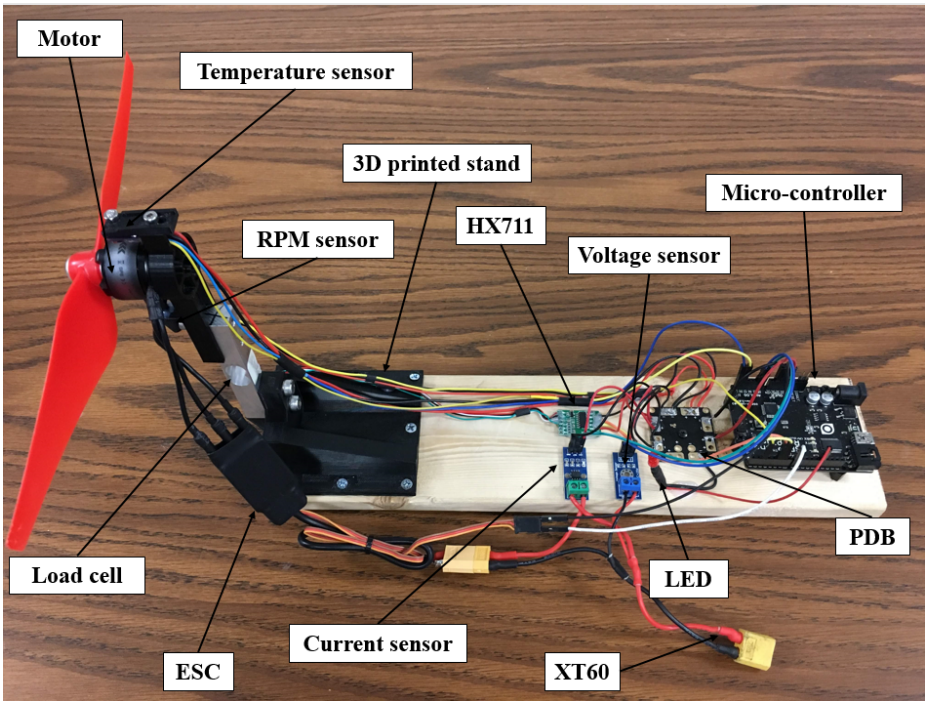

Figure 3.1: Test bench

The test bench consist of:

- Micro-controller
- 3D Printed stand
- DJI E300 Opto ESC
- Brushless motor
- Load Cell and HX711 Amplifier
- ACS712 Current Sensor
- B25 Voltage Sensor

- Optic Infra Red RPM Sensor
- MLX90615 Infra Red Temperature Sensor
- Batteries.
- Variable Voltage Power Source
- Power Distribution Board (PDB)
- XT60 connectors

The idea was not only creating a powerful and affordable RD tool for the development of this thesis, but also for other users in the future. This platform is flexible and allows the user to design personalized experiments and modify a wide range of experiment parameters. The prototype was built by the author during the realization of the thesis, but a second version is being developed for his personal use and future research. The new version features new sensors and functions.

During the experiments the purpose was emulating exactly the original quadcopter ESC-Motor-Propeller combinations installed on the multicopter. Two combinations of ESC-Motor were tested: E300-DJI-2212 and 430LITE-DJI-2312E. Both combinations where tested with different propeller models.

CHAPTER 4

EXPERIMENTAL DESIGN FOR EMPIRICAL MODELING

A set of experiments was designed and performed to obtain the ESC-Motor-Propeller functional relationship and study the variation of x, v, T, I, P, E and R in different conditions.

4.1 Variable PPM Signal at Voltage

The objective of these experiments is to determine the variation of thrust, current, power, efficiency and RPM, as a function of the PPM signal variable at constant voltage. The ESC-Motor-Propeller combination is initialized at idle speed and accelerated to the maximum speed. In the case of the DJI E300 ESC, it has the idle speed set around 1200 μs and reaches the maximum power at 1900 μs. Therefore 1200 to 1900 μs is the interval used for the experiment, increasing the PPM signal by 5 μs every iteration. Tests were run at constant voltage. From 10.5 volts to 12.6 increasing 0.3 volts in each experiment.

4.1.1 Experiment Results

The results of the variable PPM signal at constant voltage experiments are package of data containing the MATLAB workspace, different plots and a table. This table contains the values of time, PPM, current, voltage, power, efficiency, RPM, room temperature and motor temperature.

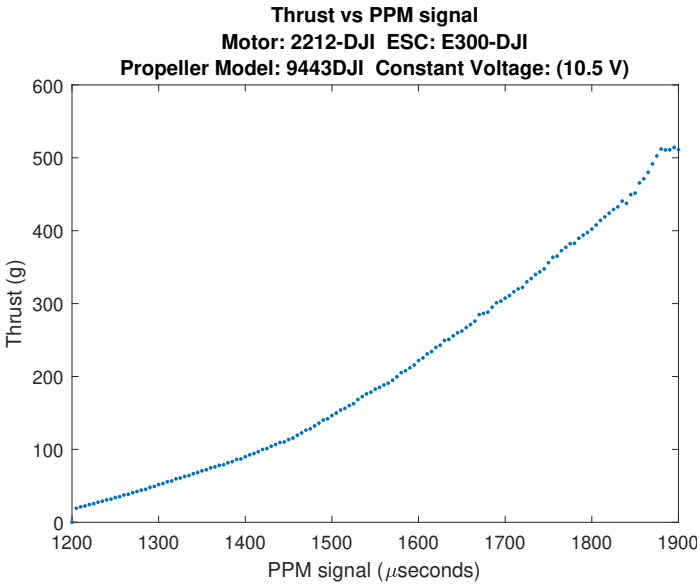

Figure 4.1: Thrust vs PPM

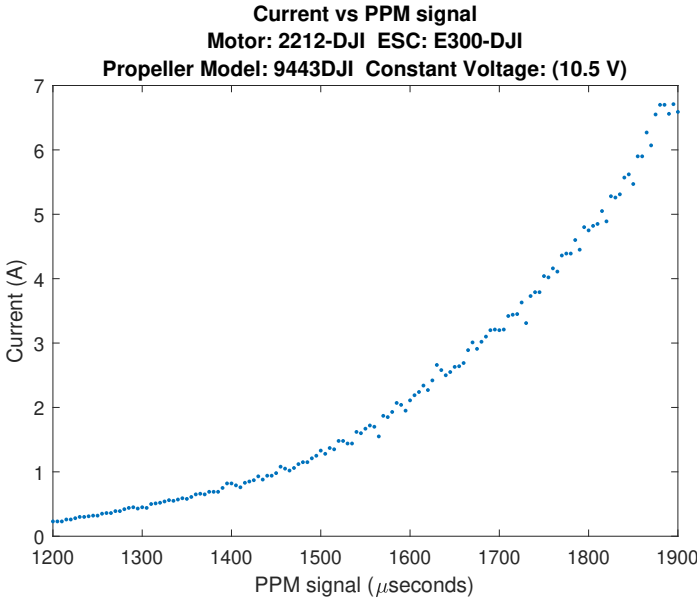

Figure 4.2: Current vs PPM

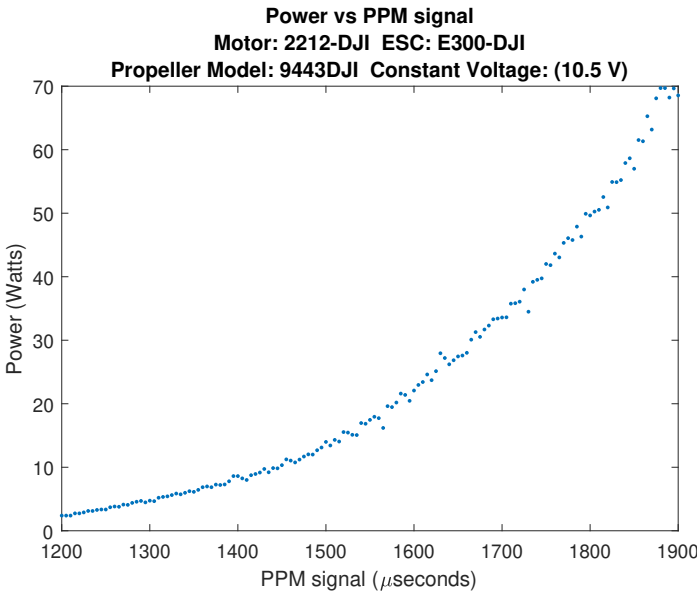

Figure 4.3: Power vs PPM

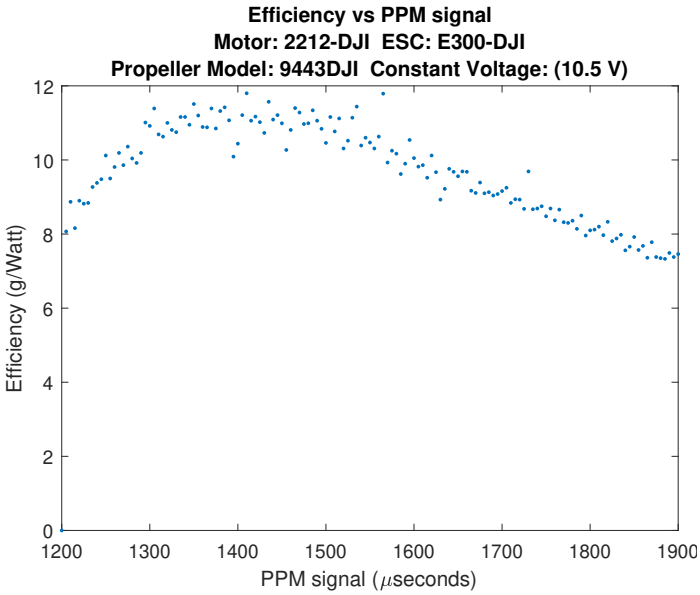

Figure 4.4: Efficiency vs PPM

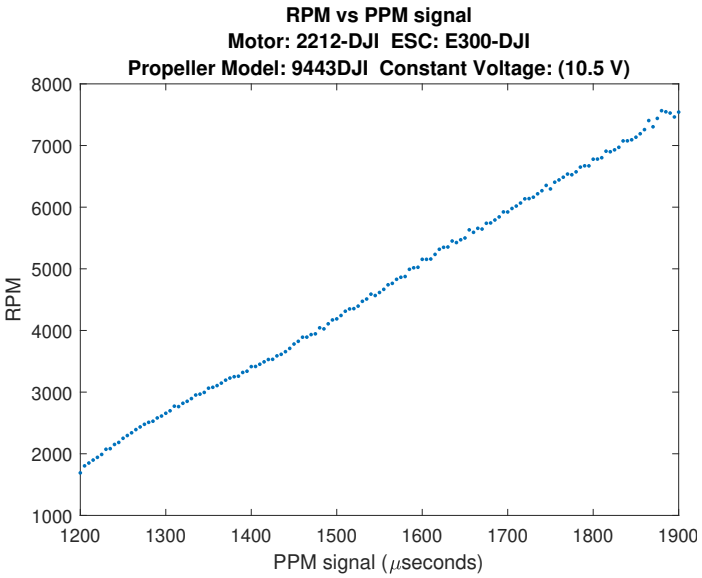

Figure 4.5: Rpm vs PPM

Note that temperature is growing with the increase PPM signal, but is not a strictly a function of it. It depends on other factors too. For example, the propeller model, time of the experiment, room temperature and others. Therefore, a functional representation of the motor temperature is out of the scope of this research. Temperature measurements in all the experiments in order to track the values and check if there is overheating of the motor at certain high power regimes, with certain propeller models. What is interesting for this research is the maximum temperature reached during the test, and checking that it is not exceeding certain values.

Temperature graphs could be presented with respect to the PPM signal as shown in figure 4.6

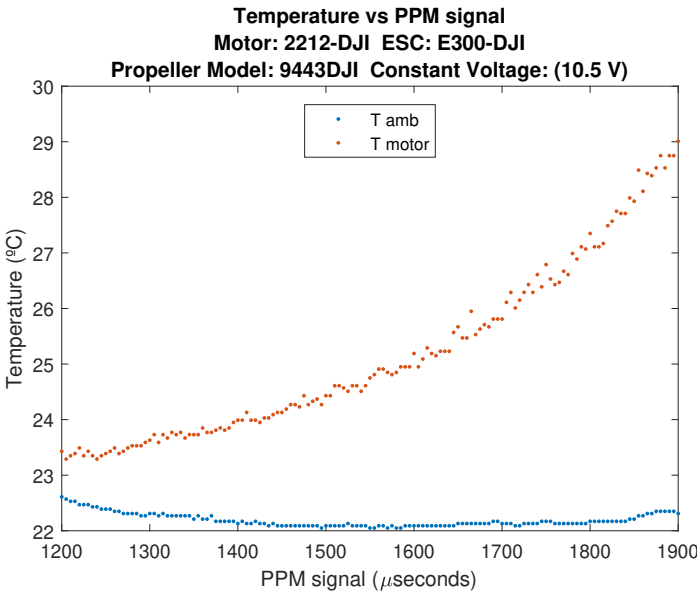

Figure 4.6: Temperature vs PPM

Or with respect to the experiment time as shown in figure 4.7

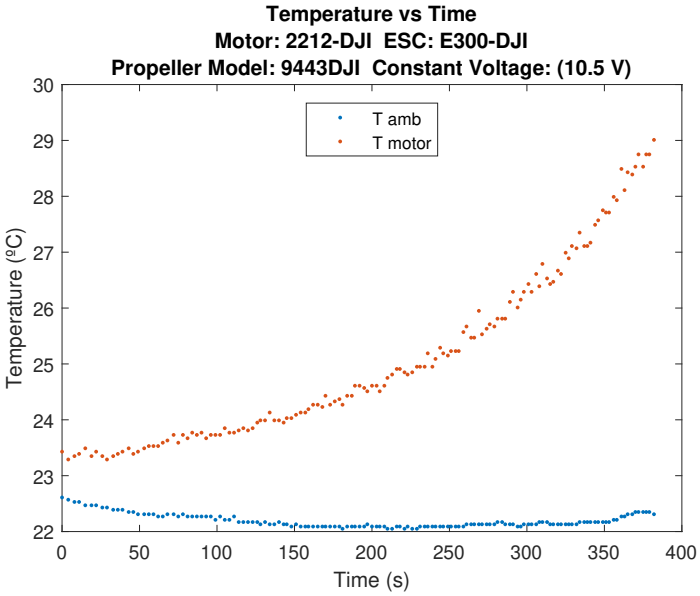

Figure 4.7: Temperature vs Time

4.1.2 Data Curve Approximation

Once the data was obtained from the variable PPM signal at constant voltage tests, MATLAB Curve Fitting Toolbox version 3.5.6 package was used to perform the curve fitting. This is a powerful tool that allows the user to fit different types of curves and surfaces to a data set. As mentioned before, there are eight sets of data per dependent variable (Thrust, Current, Power, Efficiency, RPM), corresponding to 10.5, 10.8, 11.1, 11.4, 11.7, 12.0, 12.3 and 12.6 V.

4.1.2.1 Functional Representation of Thrust vs PPM signal at Constant Voltage

As shown in figure 4.8, the thrust vs PPM signal data set distribution can be approximated as a parabolic function:

$$T(x) = p_2 x^2 + p_1 x + p_0 \tag{4.1}$$

where T is the thrust in grams and x is PPM signal in μs. The values for p_2, p_1 and p_0 are shown in table 4.1

Table 4.1: Thrust vs PPM at constant voltage

Item	**Value**
p_2	7.174×10^{-4}
p_1	-1.508
p_0	797

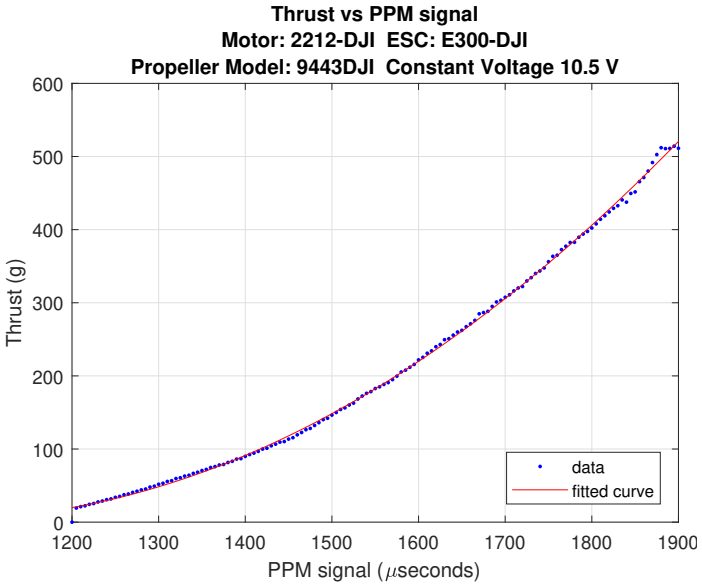

Figure 4.8: Thrust vs PPM for 10.5 V

After performing the curve approximation to all the thrust vs PPM signal data sets, the following graph was obtained:

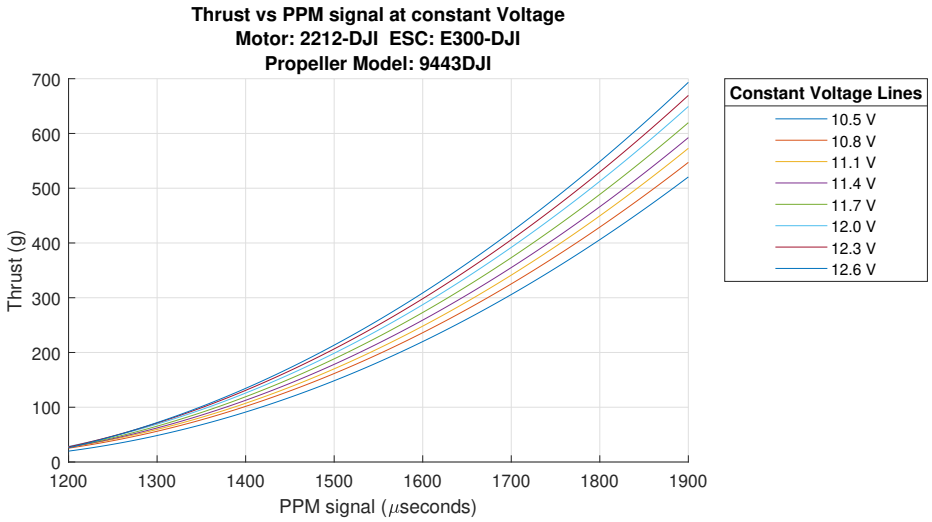

Figure 4.9: Thrust vs PPM at constant voltage

4.1.2.2 Functional Representation of Current vs PPM signal at Constant Voltage

In this case, as shown in figure 4.10, the current vs PPM signal data set distribution can be approximated as a cubic function:

$$I(x) = p_3x^3 + p_2x^2 + p_1x + p_0 \tag{4.2}$$

where I is the current in amps and x is PPM signal in μs. The values for p_3, p_2, p_1 and p_0 are shown in table 4.2

Table 4.2: Current vs PPM at constant voltage

Item	**Value**
p_3	1.235×10^{-8}
p_2	-4.213 $\times 10^{-5}$
p_1	0.04948
p_0	-19.81

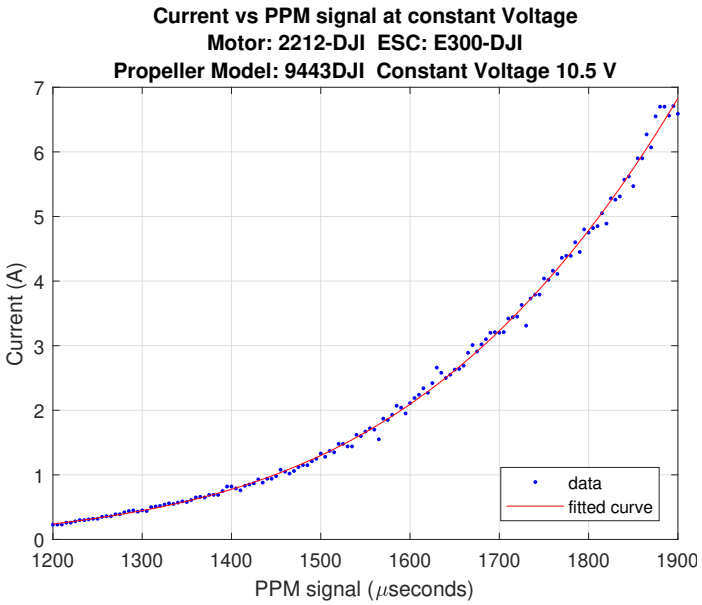

Figure 4.10: Current vs PPM for 10.5 V

After performing the curve approximation to all the current vs PPM signal data sets, the following graph was obtained:

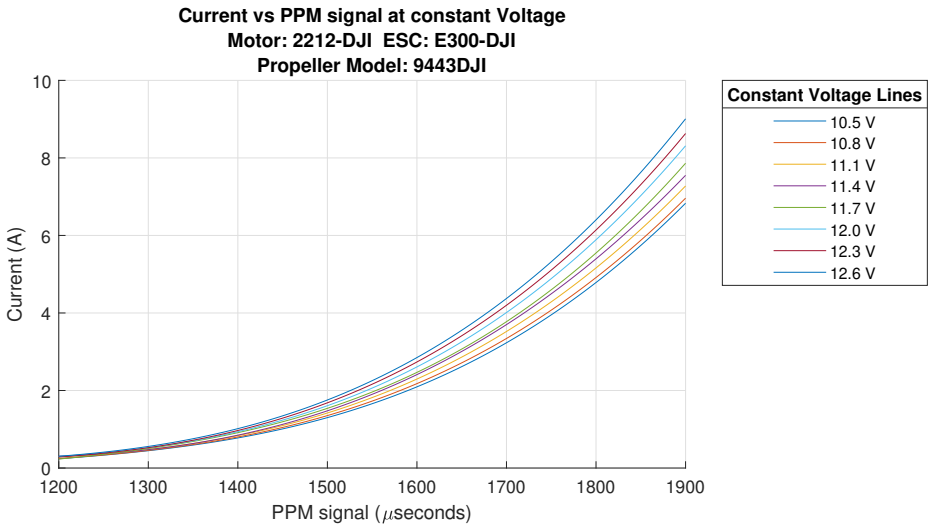

Figure 4.11: Current vs PPM at constant voltage

4.1.2.3 Functional Representation of Power vs PPM signal at Constant Voltage

In the same way, as shown in figure 4.12, the power vs PPM signal data set distribution can be approximated as a cubic function:

$$P(x) = p_3x^3 + p_2x^2 + p_1x + p_0 \tag{4.3}$$

where P is the power in watts and x is PPM signal in μs. The values for p_3, p_2, p_1 and p_0 are shown in table 4.3

Table 4.3: Power vs PPM at constant voltage

Item	Value
p_3	1.247×10^{-7}
p_2	-4.217 $\times 10^{-4}$
p_1	0.4911
p_0	-195

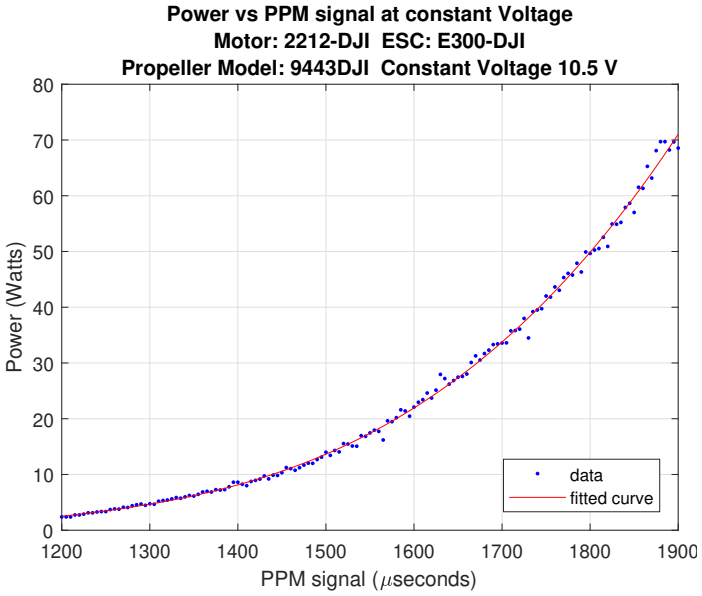

Figure 4.12: Power vs PPM for 10.5 V

After performing the curve approximation to all the power vs PPM signal data sets, the following graph was obtained:

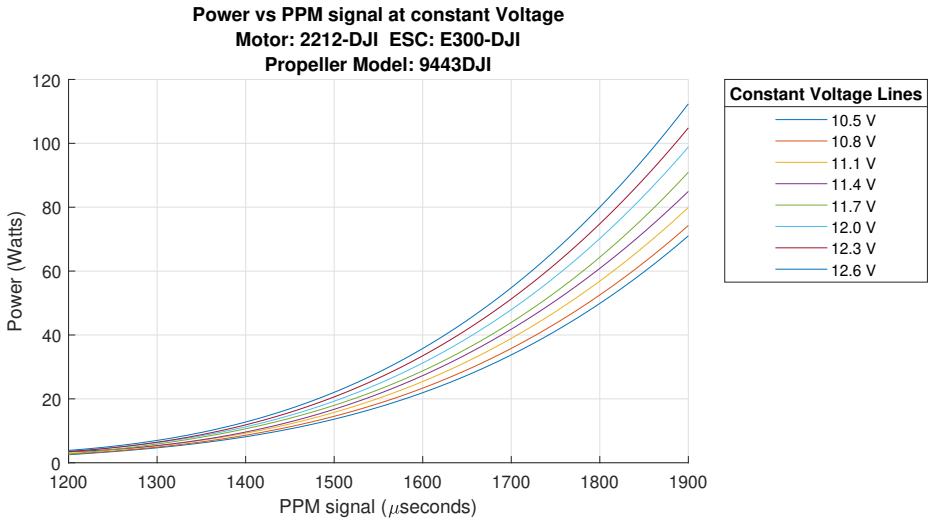

Figure 4.13: Power vs PPM at constant voltage

4.1.2.4 Functional Representation of Efficiency vs PPM signal at Constant Voltage

In the case of the efficiency vs PPM signal data, neither of the previous quadratic nor cubic function fitted correctly the data distribution. After trying several models, as shown in figure 4.14, the best fit was a rational function of second order in the numerator and third order in the denominator:

$$E(x) = \frac{p_2x^2 + p_1x + p_0}{q_3x^3 + q_2x^2 + q_1x + q_0} \tag{4.4}$$

where E is the efficiency in g/watts and x is PPM signal in μs. The values for p_2, p_1, p_0, q_3, q_2, q_1 and q_0 are shown in table 4.4

Table 4.4: Efficiency vs PPM at constant voltage

Item	Value
p_2	2021
p_1	-1.514 $\times$ 10^5
p_0	-295.5
q_3	1
q_2	-2719
q_1	2.09 $\times$ 10^6
q_0	3736

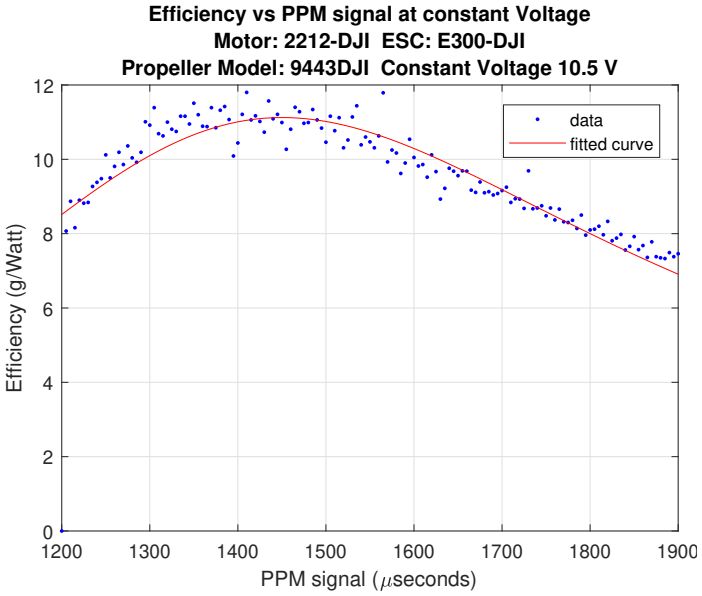

Figure 4.14: Efficiency vs PPM for 10.5 V

After performing the curve approximation to all the efficiency vs PPM signal data sets, the following graph was obtained:

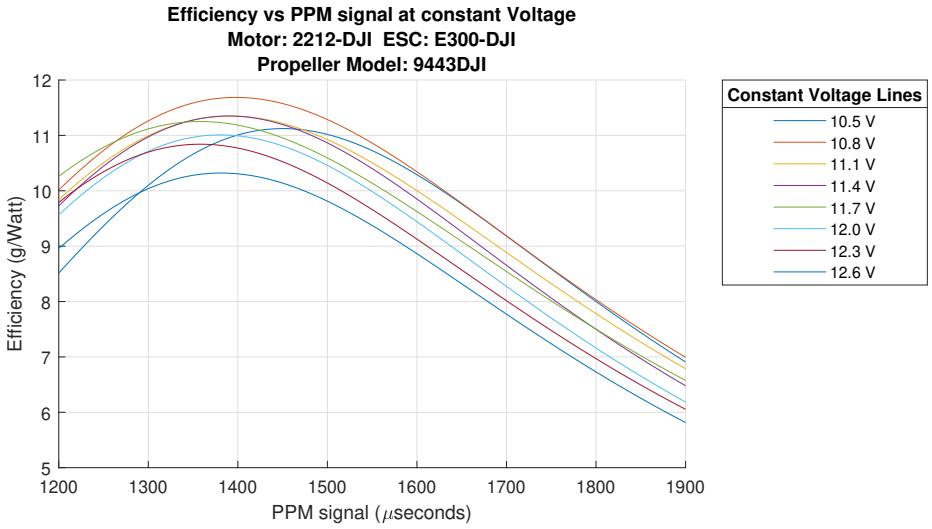

Figure 4.15: Efficiency vs PPM at constant voltage

4.1.2.5 Functional Representation of RPM vs PPM signal at Constant Voltage

Finally, in figure 4.16, RPM vs PPM signal distribution was fitted to a linear function:

$$R(x) = p_1 x + p_0 \tag{4.5}$$

where R is RPM and x is PPM signal in μs. The values for p_1 and p_0 are shown in table 4.5

Table 4.5: RPM vs PPM at constant voltage

Item	**Value**
p_1	8.296
p_0	-8184

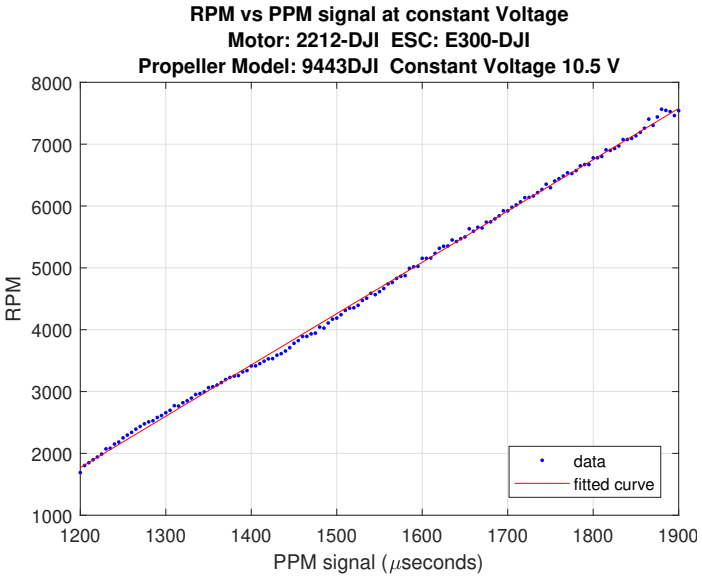

Figure 4.16: RPM vs PPM for 10.5 V

After performing the curve approximation to all the RPM vs PPM signal data sets, the following graph was obtained:

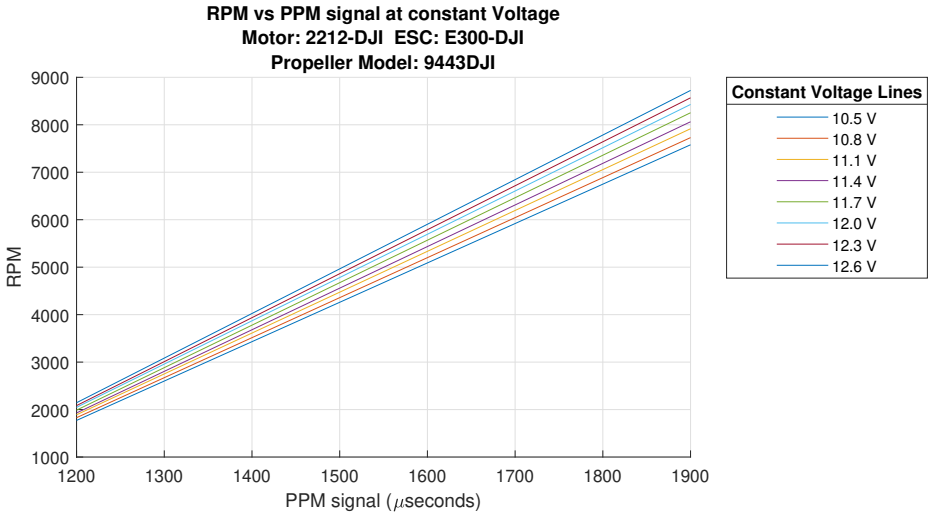

Figure 4.17: RPM vs PPM at constant voltage

4.2 Variable Voltage at Constant PPM Signal

The objective of these experiments is to study the variation of thrust, current, power, efficiency and RPM, as a function of the voltage at constant PPM signal. In these experiments the ESC-Motor-Propeller combination is initialized at a known PPM signal, that will remain constant during the experiment. Voltage decreases from 12.60 V (full charged battery) to 10.50 V (discharged battery). When the voltage drops below 10.5 V the experiment stops. The higher the PPM signal value is, the shorter the experiment will be.

4.2.1 Experiment Results

The results of the variable voltage at constant PPM signal tests are package of data containing the MATLAB workspace, different plots and a table. This table contains values of time, PPM, current, voltage, power, efficiency, RPM, room temperature and motor temperature.

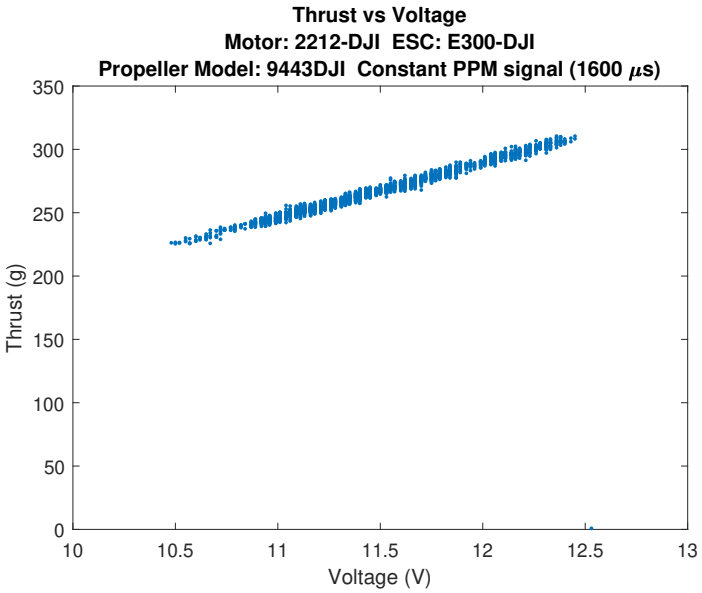

Figure 4.18: Thrust vs voltage

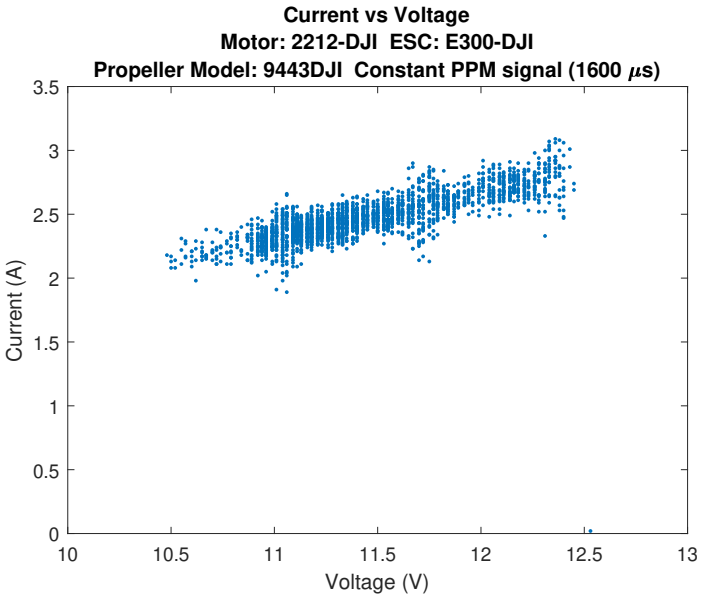

Figure 4.19: Current vs voltage

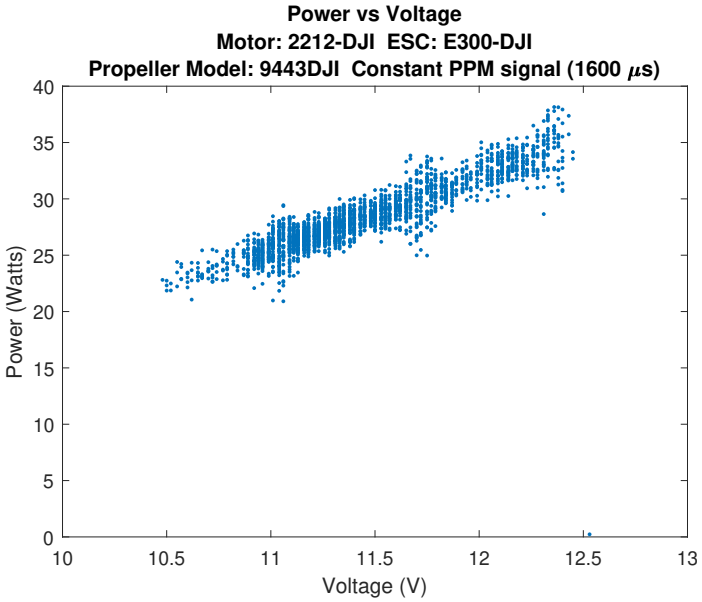

Figure 4.20: Power vs voltage

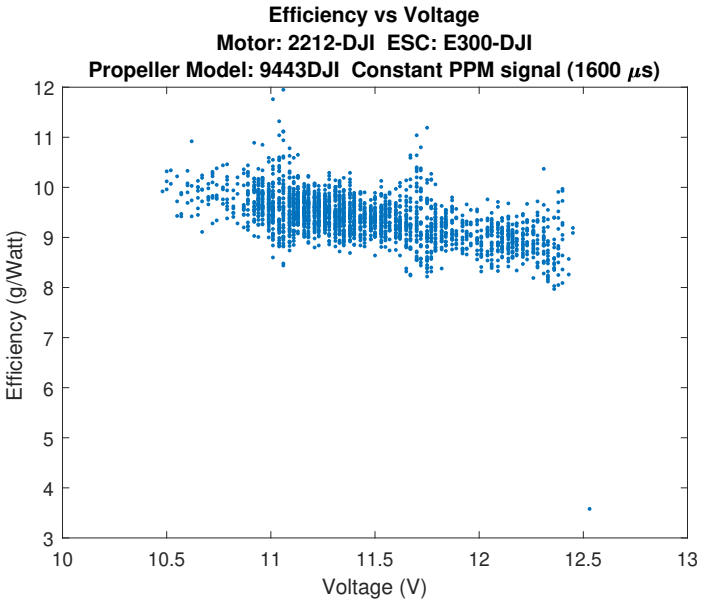

Figure 4.21: Efficiency vs voltage

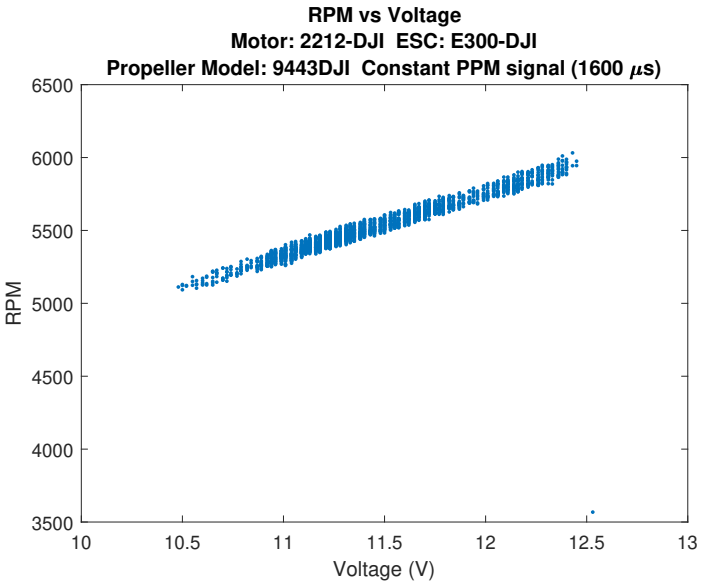

Figure 4.22: RPM vs voltage

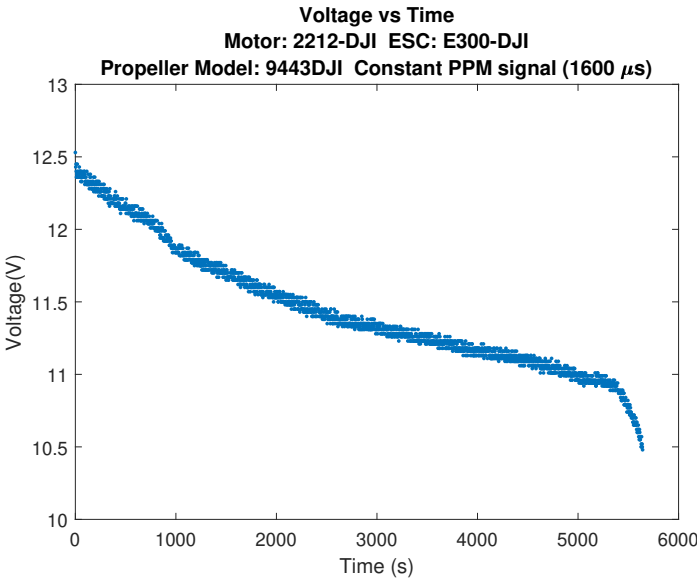

Figure 4.23: Voltage vs time

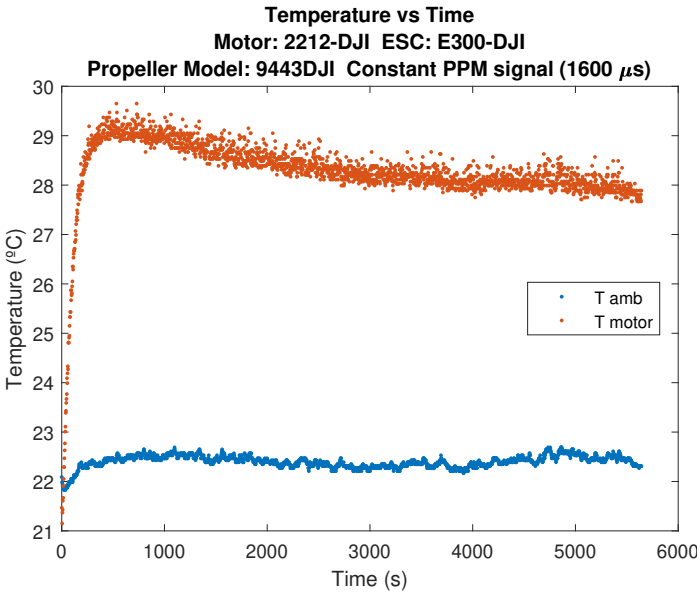

Figure 4.24: Temperature vs time

4.2.2 Data Curve Approximation

Once the data was obtained from the variable voltage at constant PPM signal experiments, a process of curve fitting was performed. This time, there are four sets of data per dependent variable (Thrust, Current, Power, Efficiency, RPM), corresponding to 1600,1700,1800 and 1900 μs of constant PPM signal. The behavior of all the variables resulted to be linear, except the voltage as a function of the time.

4.2.2.1 Functional Representation of Thrust vs Voltage at Constant PPM Signal

As shown in figure 4.25, thrust vs voltage data is fitted to a linear function:

$$T(v) = p_1 v + p_0 \tag{4.6}$$

where T is the thrust in grams and v is the voltage in volts. The values for p_1 and p_0 are shown in table 4.6

Table 4.6: Thrust vs voltage at constant PPM

Item	**Value**
p_1	42.62
p_0	-222.5

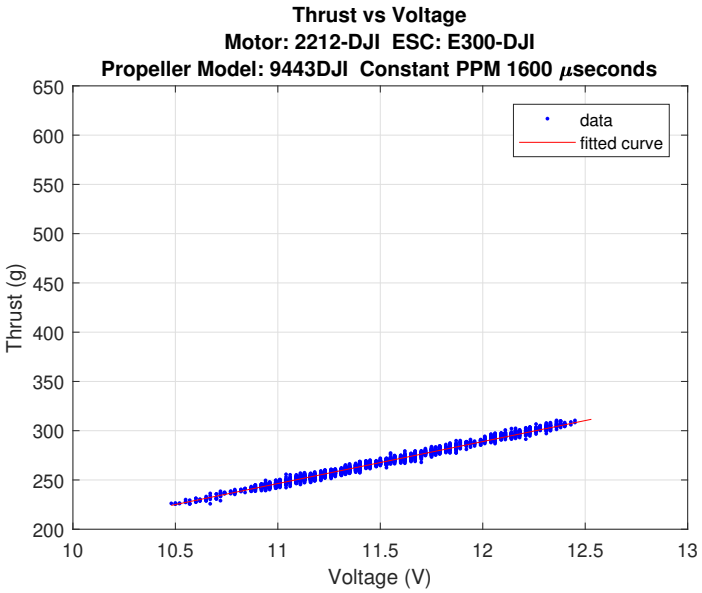

Figure 4.25: Thrust vs voltage for 1600 μs

After performing the linear function approximation to all the thrust vs voltage at constant PPM signal data sets, the following graph was obtained:

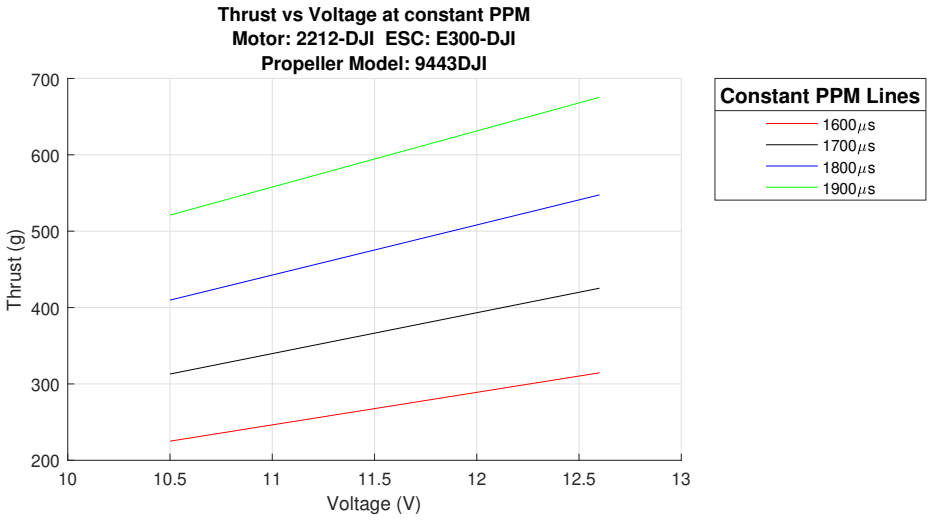

Figure 4.26: Thrust vs voltage at constant PPM

4.2.2.2 Functional Representation of Current vs Voltage at Constant PPM Signal

As shown in figure 4.27, current vs voltage data is fitted to a linear function:

$$I(v) = p_1 v + p_0 \tag{4.7}$$

where I is the current in amps and v is the voltage in volts. The values for p_1 and p_0 are shown in table 4.7

Table 4.7: Current vs voltage at constant PPM

Item	Value
p_1	0.3432
p_0	-1.457

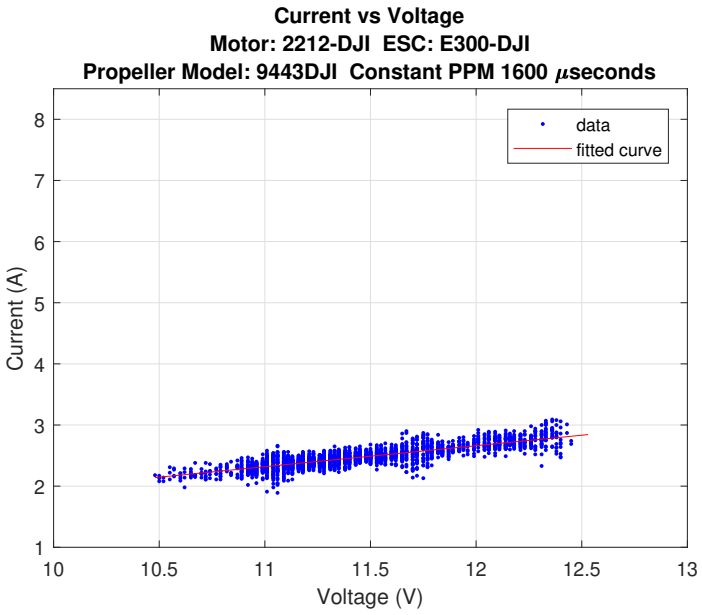

Figure 4.27: Current vs voltage for 1600 μs

After performing the linear function approximation to all the current vs voltage at constant PPM signal data sets, the following graph was obtained:

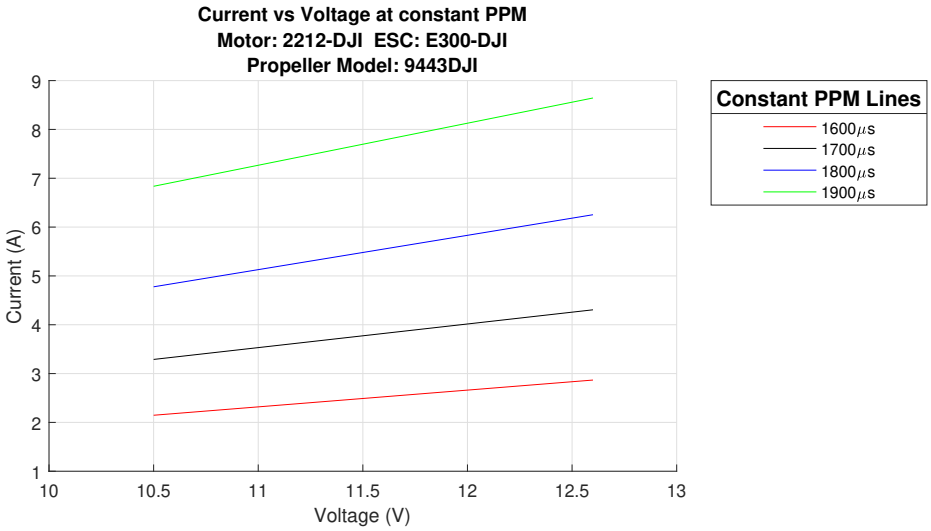

Figure 4.28: Current vs voltage at constant PPM

4.2.2.3 Functional Representation of Power vs Voltage at Constant PPM Signal

As shown in figure 4.29, power vs voltage data is fitted to a linear function:

$$P(v) = p_1 v + p_0 \tag{4.8}$$

where P is the power in watts and v is the voltage in volts. The values for p_1 and p_0 are shown in table 4.8

Table 4.8: Power vs voltage at constant PPM

Item	Value
p_1	6.469
p_2	-45.69

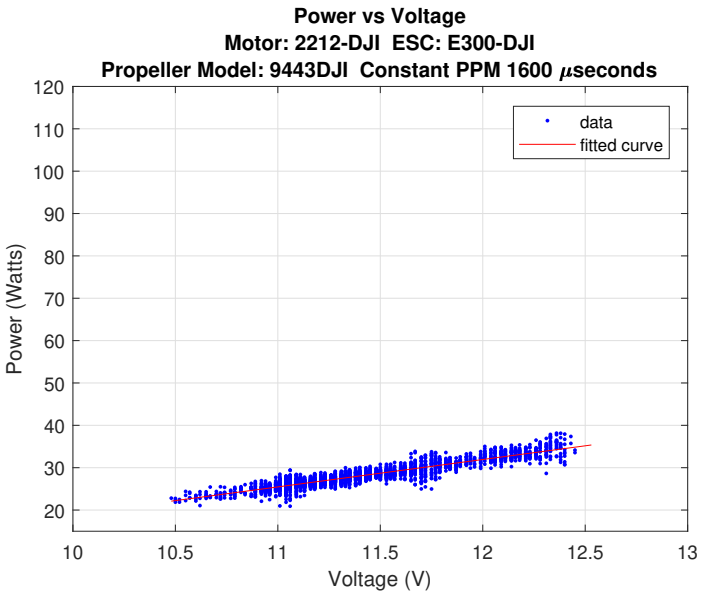

Figure 4.29: Power vs voltage for 1600 μs

After performing the linear function approximation to all the power vs voltage at constant PPM signal data sets, the following graph was obtained:

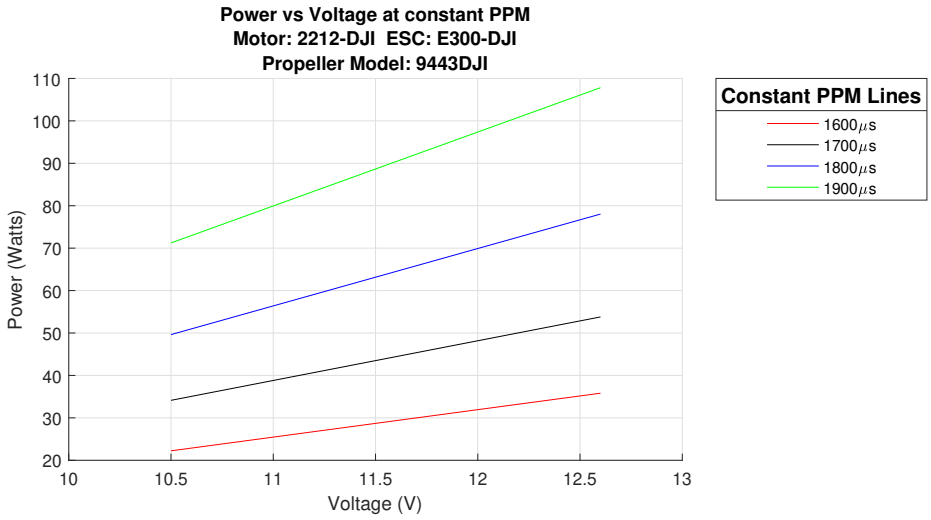

Figure 4.30: Power vs voltage at constant PPM

4.2.2.4 Functional Representation of Efficiency vs Voltage at Constant PPM Signal

As shown in figure 4.31, efficiency vs voltage data is fitted to a linear function:

$$E(v) = p_1 v + p_0 \tag{4.9}$$

where E is the efficiency in g/watts and v is the voltage in volts. The values for p_1 and p_0 are shown in table 4.9

Table 4.9: Efficiency vs voltage at constant PPM

Item	**Value**
p_1	-0.6203
p_2	16.5

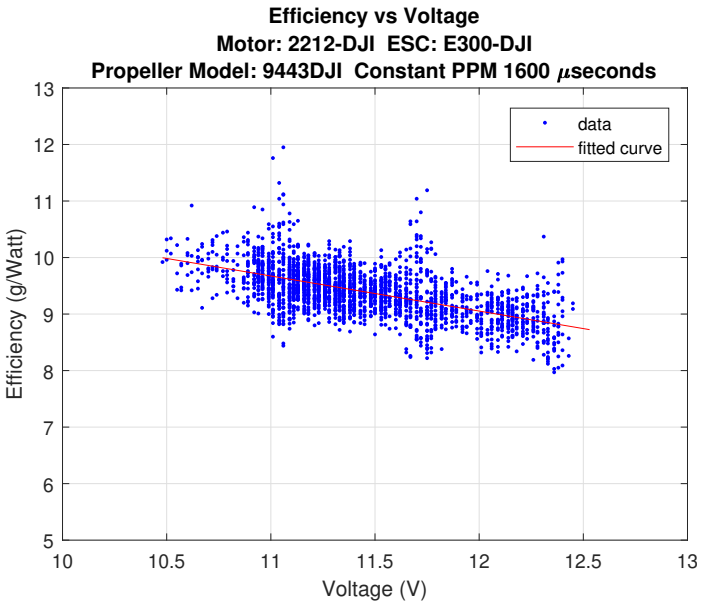

Figure 4.31: Efficiency vs voltage for 1600 μs

After performing the linear function approximation to all the efficiency vs voltage at constant PPM signal data sets, the following graph was obtained:

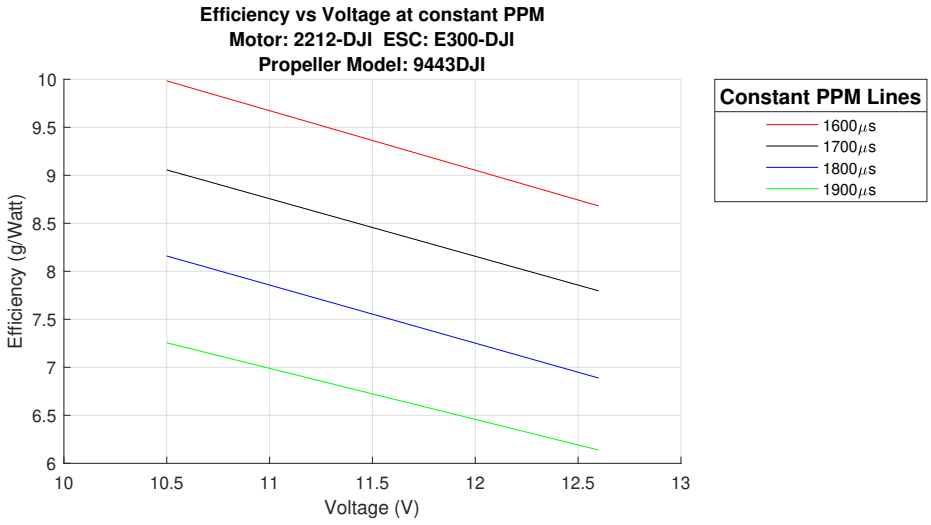

Figure 4.32: Efficiency vs voltage at constant PPM

4.2.2.5 Functional Representation of RPM vs Voltage at Constant PPM Signal Linear

As shown in figure 4.33, power vs voltage data is fitted to a linear function:

$$R(x) = p_1 v + p_0 \tag{4.10}$$

where R is RPM and v is the voltage in volts. The values for p_1 and p_0 are shown in table 4.10

Table 4.10: RPM vs voltage at constant PPM

Item	**Value**
p_1	420.7
p_2	703.9

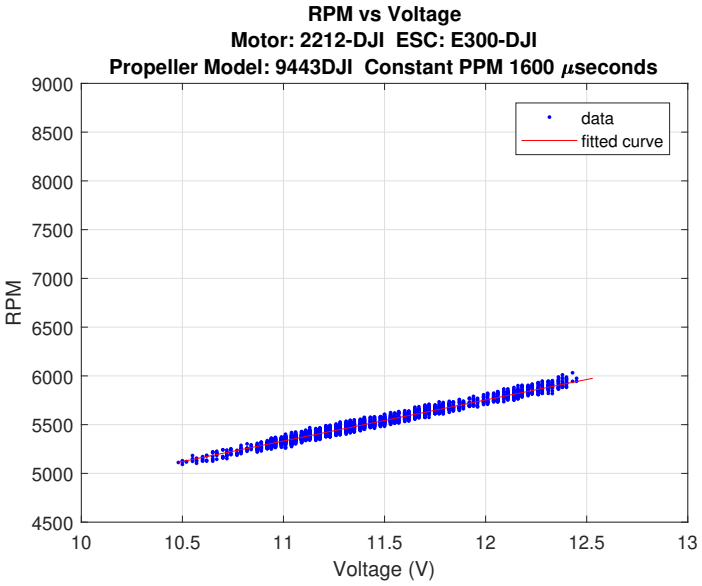

Figure 4.33: RPM vs voltage for 1600 μs

After performing the linear function approximation to all the RPM vs voltage at constant PPM signal data sets, the following graph was obtained:

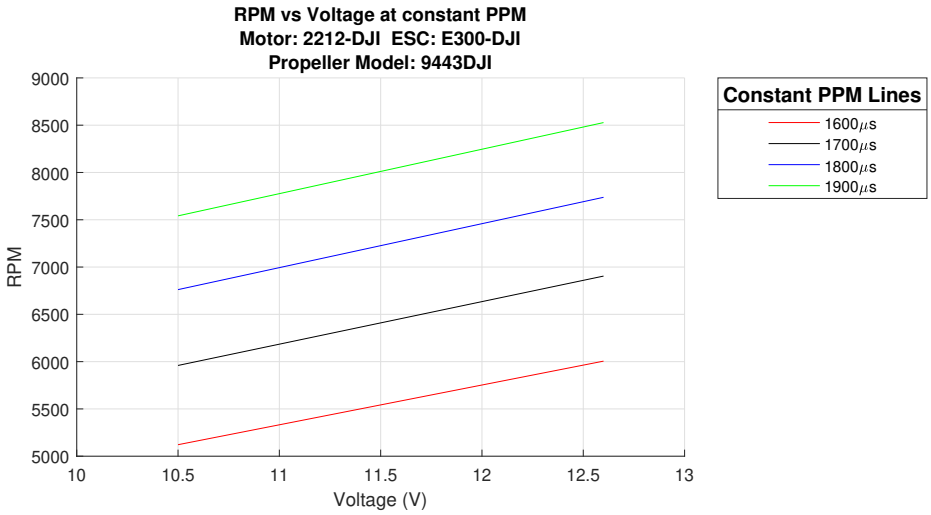

Figure 4.34: RPM vs voltage at constant PPM

4.2.2.6 Functional Representation of Voltage Drop vs Time at Constant PPM Signal

As shown in figure 4.35, voltage drop vs time data is is not a linear function. The best fit polynomial was determined as shown in equation 4.11:

$$V(t) = p_9t^9 + p_8t^8 + p_7t^7 + p_6t^6 + p_5t^5 + p_4t^4 + p_3t^3 + p_2t^2 + p_1t + p_0 \qquad (4.11)$$

where V is the voltage in volts, and t is the time in seconds. The values for p_9, p_8, p_7, p_6, p_5, p_4, p_3, p_2, p_1 and p_0 are shown in table 4.11

Table 4.11: Voltage drop vs time at constant PPM

Item	**Value**
p_9	-4.718×10^{-28}
p_8	-1.009×10^{-23}
p_7	-8.886×10^{-20}
p_6	4.13×10^{-16}
p_5	-1.099×10^{-12}
p_4	1.66×10^{-9}
p_3	-1.267×10^{-6}
p_2	-2719
p_1	1.119×10^{-4}
p_0	12.37

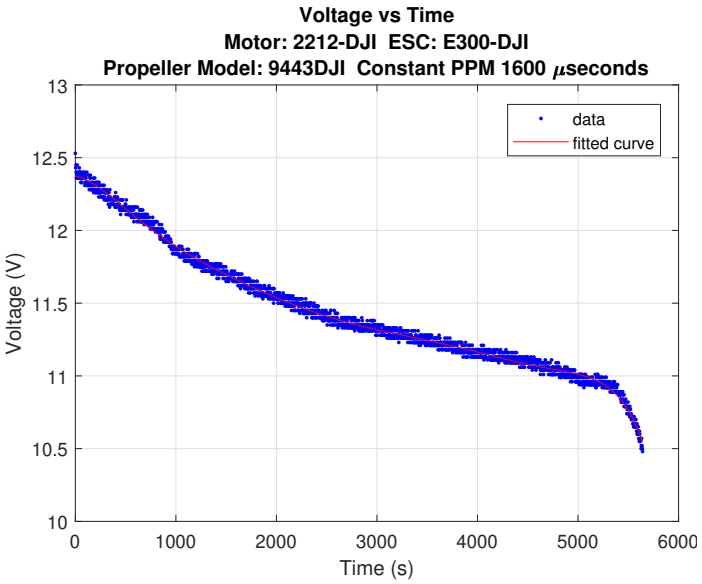

Figure 4.35: Voltage vs time for 1600 μs

After performing the curve approximation to all the voltage vs time at constant PPM signal data sets, the following graph was obtained:

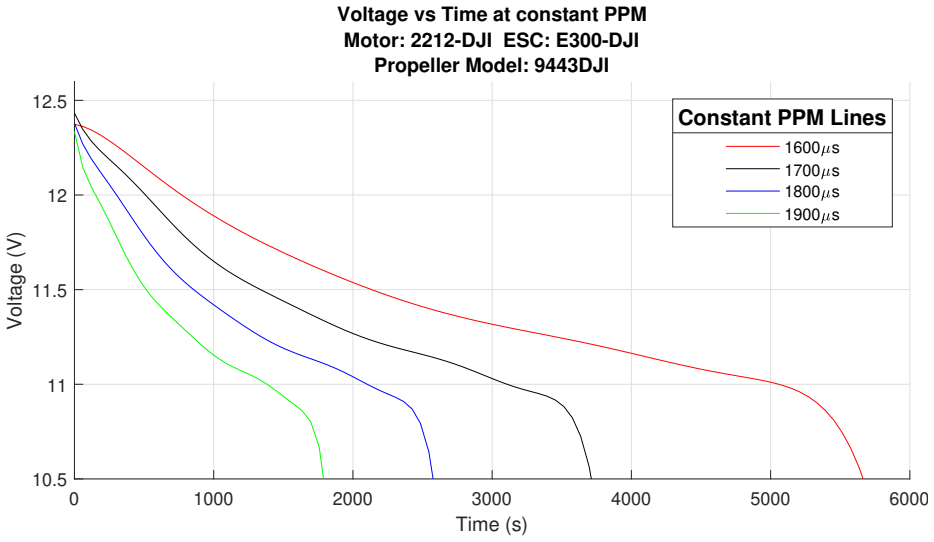

Figure 4.36: Voltage vs time at constant PPM

4.3 Variable Voltage at Constant Thrust

The objective of these experiments is to study the variation of PPM signal, current, power, efficiency and RPM, as a function of the voltage at constant thrust. In these experiments the ESC-Motor-Propeller combination is initialized at a known thrust value. A control block was implemented in the Arduino code, to adjust the PPM signal so that the thrust produced would remain constant during the experiment. In the same way that the experiment described in the previous section, voltage decreases from 12.60 V (full charged battery) to 10.50 V (discharged battery). When the voltage drops below 10.5 V the experiment stops. The higher the PPM signal value is, the shorter the experiment will be.

4.3.1 Experiment Results

The results of the variable voltage at constant thrust tests are package of data containing the MATLAB workspace, different plots and a table. This table contains values of time, PPM, current, voltage, power, efficiency, RPM, room temperature and motor temperature.

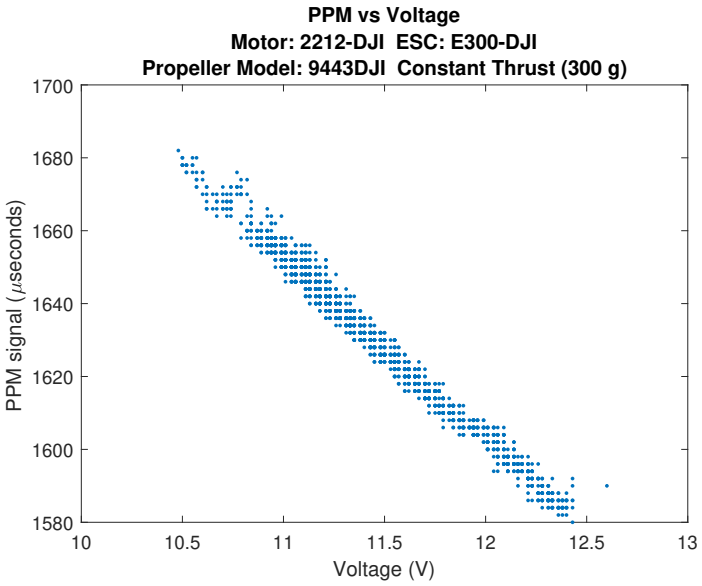

Figure 4.37: PPM vs voltage

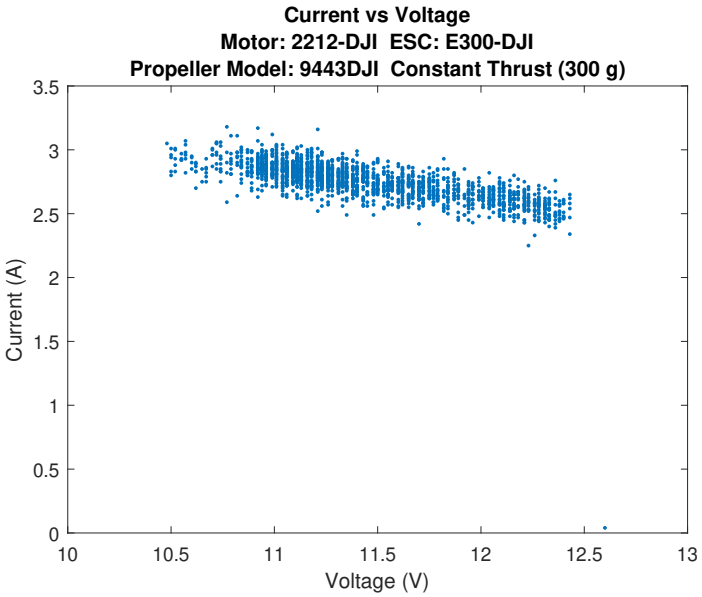

Figure 4.38: Current vs voltage

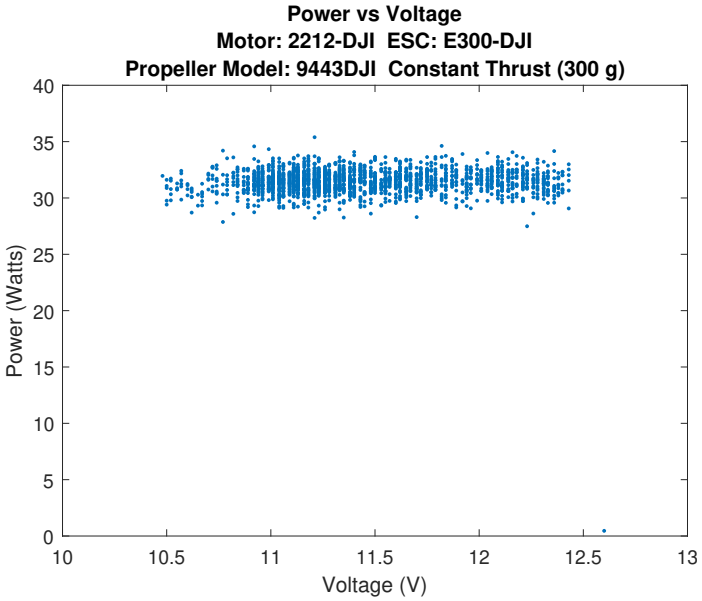

Figure 4.39: Power vs voltage

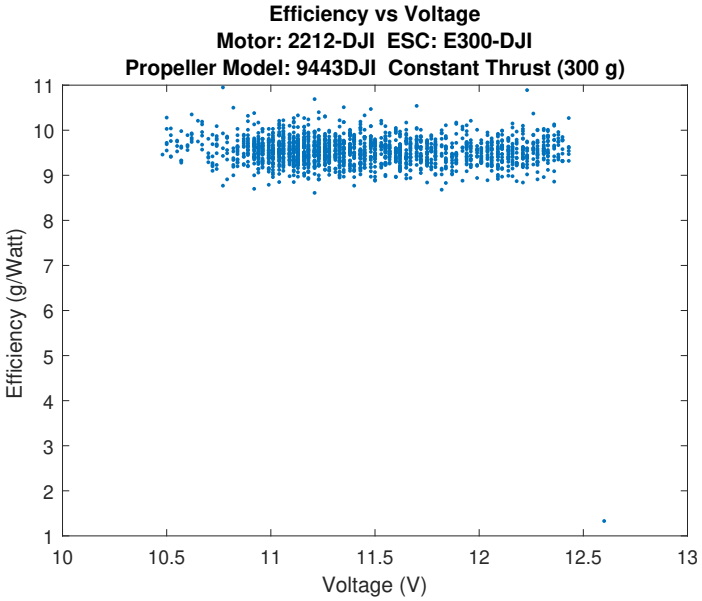

Figure 4.40: Efficiency vs voltage

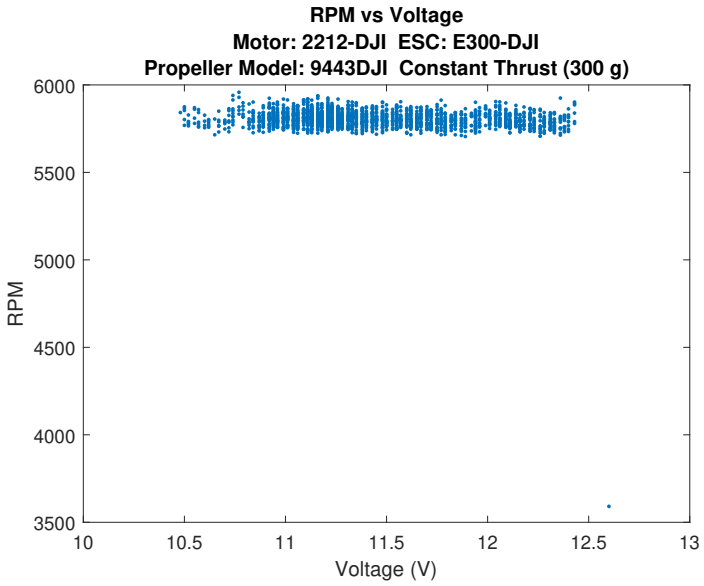

Figure 4.41: RPM vs voltage

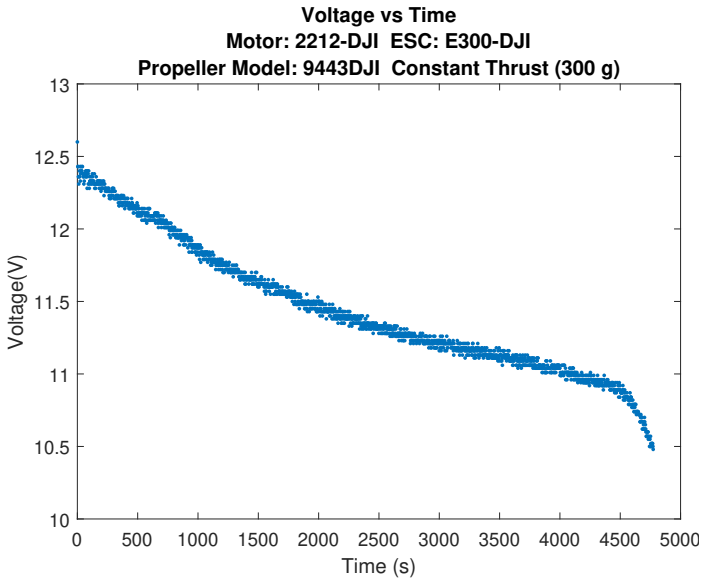

Figure 4.42: Voltage vs time

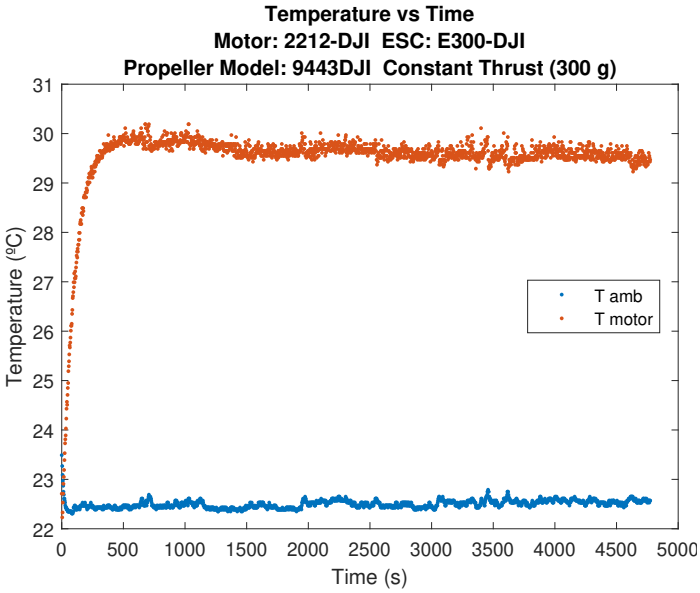

Figure 4.43: Temperature vs time

4.3.2 Data Curve Approximation

Once the data was obtained from the variable voltage at constant thrust experiments, a process of curve fitting was performed. There are four sets of data per dependent variable (PPM signal, Current, Power, Efficiency, RPM), corresponding to 300, 350, 400, 450 and 500 μs of constant thrust. As in the previous experiments, the behavior of all the variables resulted to be linear, except the voltage as a function of the time.

4.3.2.1 Functional Representation of PPM Signal vs Voltage at Constant Thrust

As shown in figure 4.44, PPM signal vs voltage data is fitted to a linear function:

$$X(v) = p_1 v + p_0 \tag{4.12}$$

where X is the PPM signal in μs and v is the voltage in volts. The values for p_1 and p_0 are shown in table 4.12

Table 4.12: PPM vs voltage at constant thrust

Item	Value
p_1	-50.11
p_0	2204

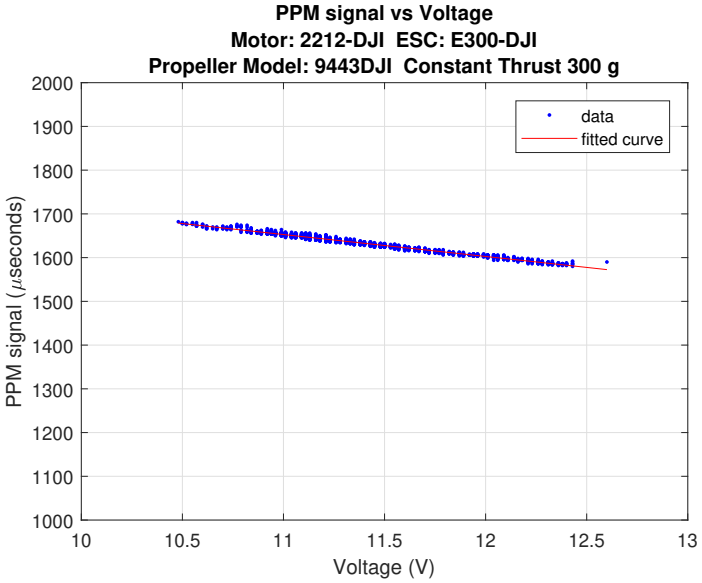

Figure 4.44: PPM signal vs voltage for 300 g

After performing the linear function approximation to all the PPM signal vs voltage at constant thrust data sets, the following graph was obtained:

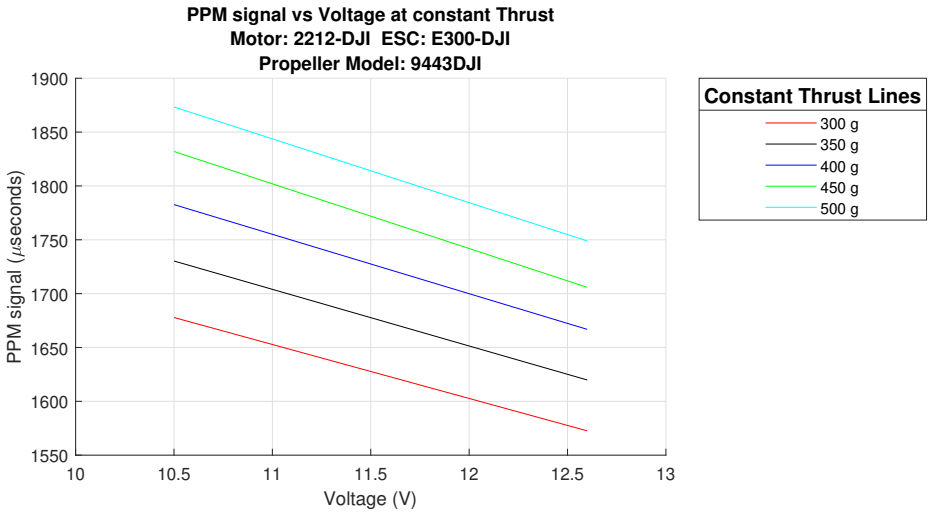

Figure 4.45: PPM signal vs voltage at constant thrust

4.3.2.2 Functional Representation of Current vs Voltage at Constant Thrust

As shown in figure 4.46, current vs voltage data is fitted to a linear function:

$$I(v) = p_1 v + p_0 \tag{4.13}$$

where I is the current in amps and v is the voltage in volts. The values for p_1 and p_0 are shown in table 4.13

Table 4.13: Current vs voltage at constant thrust

Item	**Value**
p_1	-0.2325
p_0	5.413

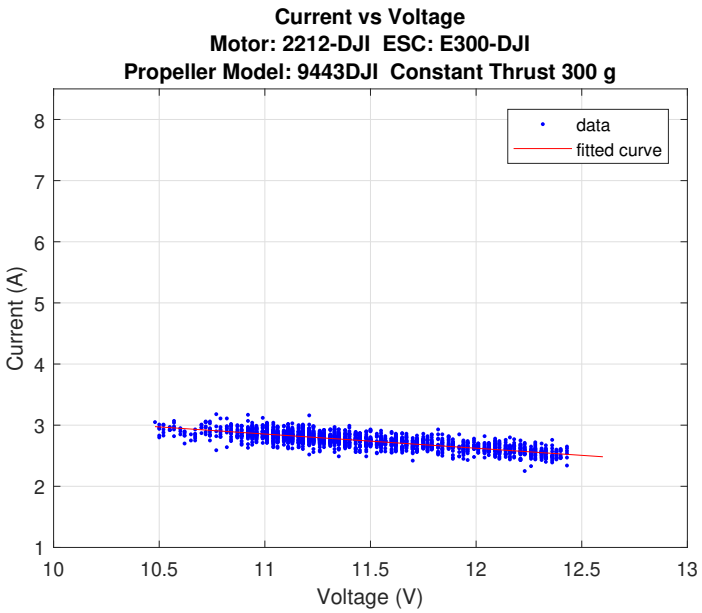

Figure 4.46: Current vs voltage for 300 g

After performing the linear function approximation to all the current vs voltage at constant thrust data sets, the following graph was obtained:

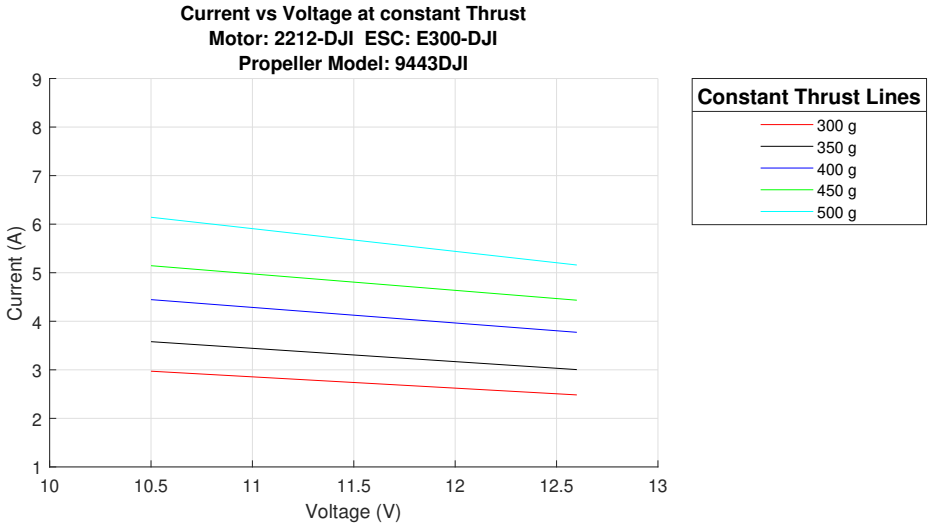

Figure 4.47: Current vs voltage at constant thrust

4.3.2.3 Functional Representation of Power vs Voltage at Constant Thrust

As shown in figure 4.48, power vs voltage data is fitted to a linear function:

$$P(v) = p_1 v + p_0 \tag{4.14}$$

where P is the power in watts and v is the voltage in volts. The values for p_1 and p_0 are shown in table 4.14

Table 4.14: Power vs voltage at constant thrust

Item	Value
p_1	0.03628
p_2	31.03

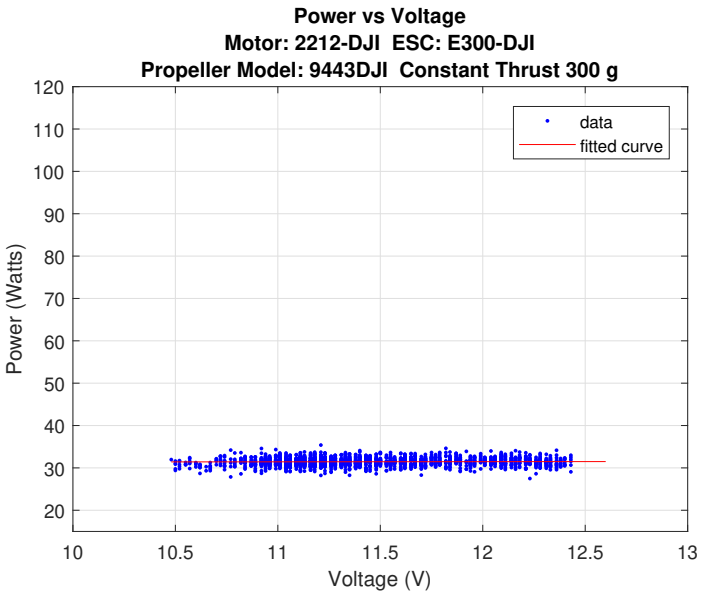

Figure 4.48: Power vs voltage for 300 g

After performing the linear function approximation to all the power vs voltage at constant thrust data sets, the following graph was obtained:

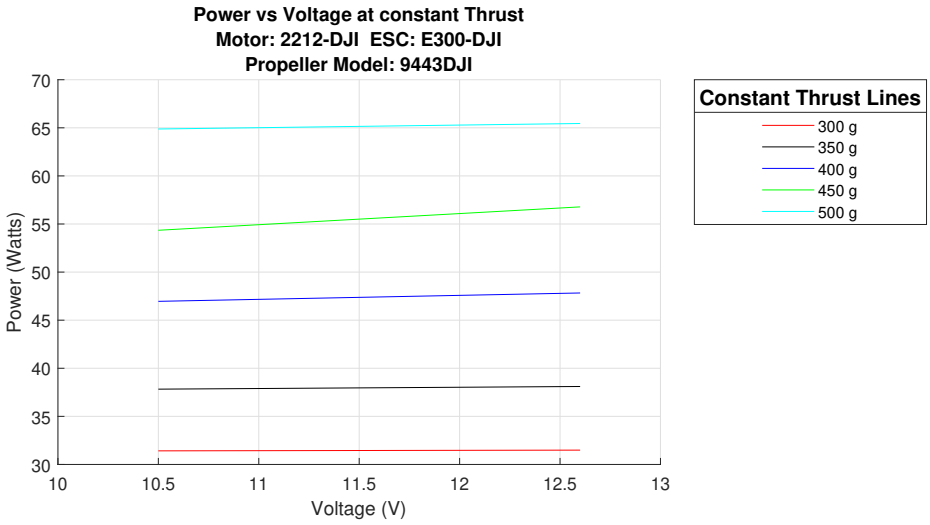

Figure 4.49: Power vs voltage at constant thrust

4.3.2.4 Functional Representation of Efficiency vs Voltage at Constant Thrust

As shown in figure 4.50, efficiency vs voltage data is fitted to a linear function:

$$E(v) = p_1 v + p_0 \tag{4.15}$$

where E is the efficiency in g/watts and v is the voltage in volts. The values for p_1 and p_0 are shown in table 4.15

Table 4.15: Efficiency vs voltage at constant thrust

Item	**Value**
p_1	-0.06382
p_2	10.27

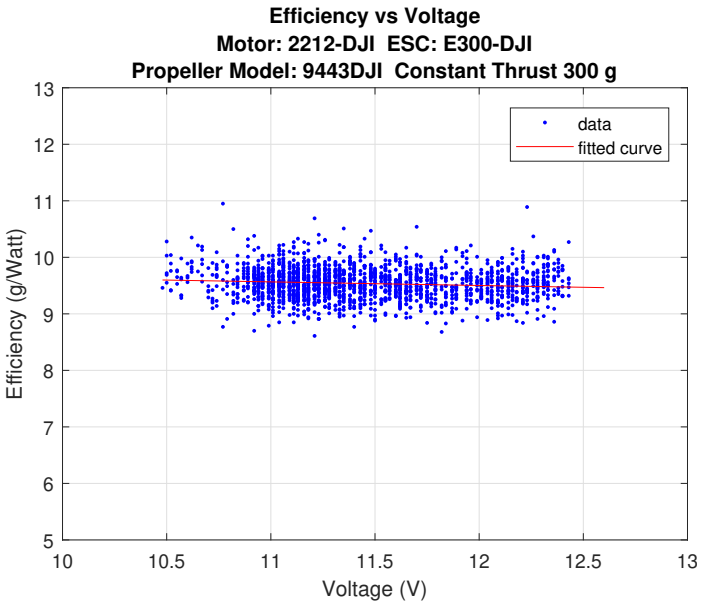

Figure 4.50: Efficiency vs voltage for 300 g

After performing the linear function approximation to all the efficiency vs voltage at constant thrust data sets, the following graph was obtained:

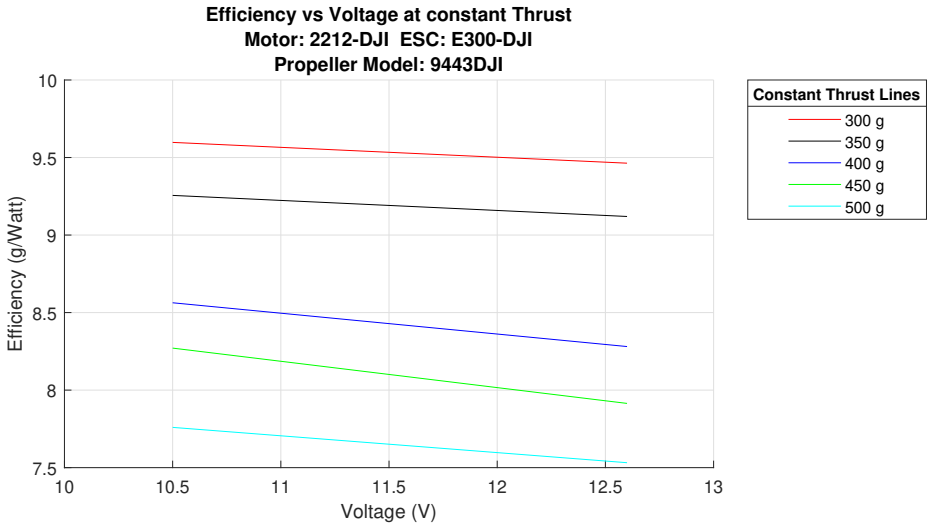

Figure 4.51: Efficiency vs voltage at constant thrust

4.3.2.5 Functional Representation of RPM vs Voltage at Constant Thrust

As shown in figure 4.52, power vs voltage data is fitted to a linear function:

$$R(x) = p_1 v + p_0 \tag{4.16}$$

where R is RPM and v is the voltage in volts. The values for p_1 and p_0 are shown in table 4.16

Table 4.16: RPM vs voltage at constant thrust

Item	Value
p_1	-22.23
p_2	6059

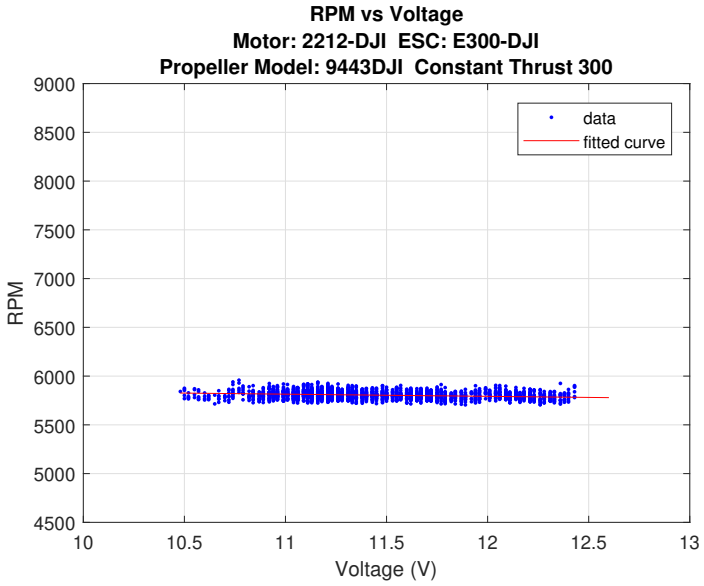

Figure 4.52: RPM vs voltage for 300 g

After performing the linear function approximation to all the RPM vs voltage at constant thrust data sets, the following graph was obtained:

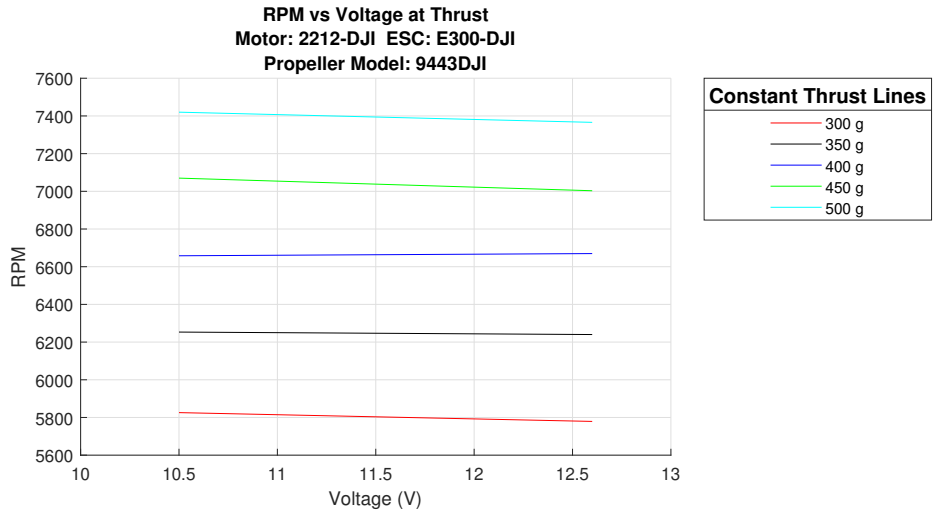

Figure 4.53: RPM vs voltage at constant thrust fitted lines graph

4.3.2.6 Functional Representation of Voltage Drop vs Time at Constant Thrust

As shown in figure 4.54, voltage vs time data is is not a linear function. It has to be fitted to a curve. After trying polynomial models of different orders, the best fit is a ninth order polynomial function of the form:

$$V(t) = p_8 t^8 + p_7 t^7 + p_6 t^6 + p_5 t^5 + p_4 t^4 + p_3 t^3 + p_2 t^2 + p_1 t + p_0 \tag{4.17}$$

where V is the drop voltage in volts, and t is the time in seconds. The values for p_8, p_7, p_6, p_5, p_4, p_3, p_2, p_1 and p_0 are shown in table 4.17

Table 4.17: Voltage drop vs time at constant thrust

Item	Value
p_8	-8.875×10^{-28}
p_7	1.497×10^{-23}
p_6	-1.029×10^{-16}
p_5	3.739×10^{-16}
p_4	-7.85×10^{-13}
p_3	9.9×10^{-10}
p_2	-6.65×10^{-7}
p_1	-3.516×10^{-4}
p_0	12.39

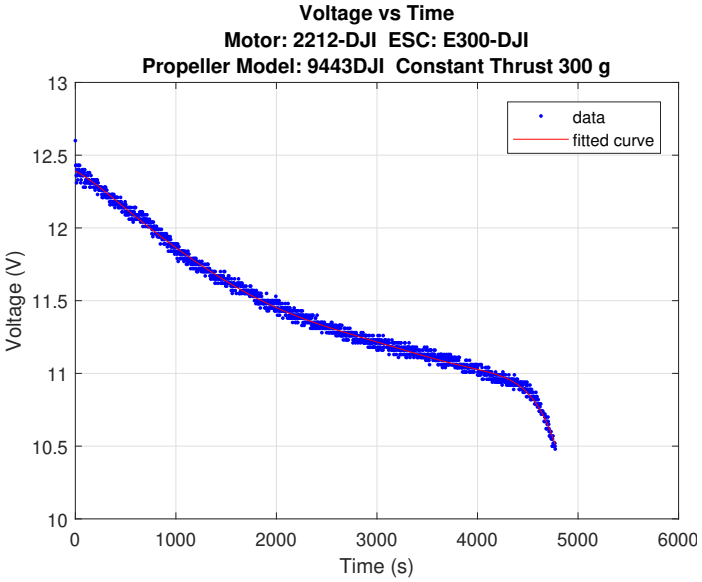

Figure 4.54: Voltage vs time for 300 g

After performing the curve approximation to all the voltage vs time at constant thrust data sets, the following graph was obtained:

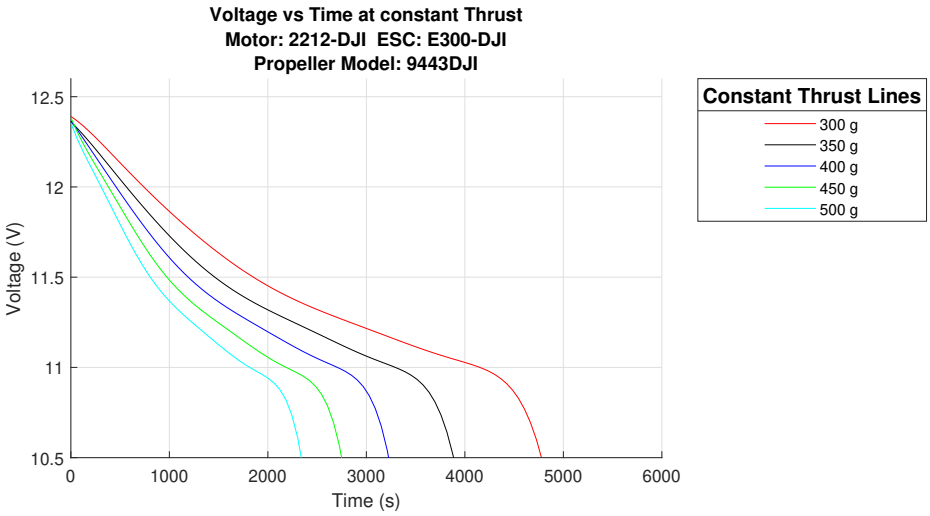

Figure 4.55: Voltage vs time at constant thrust

CHAPTER 5

EMPIRICAL MODELING

After studying the behavior of thrust, current, power, efficiency and RPM with respect to PPM signal and voltage separately, in this section, the variation of these parameters will be studied with respect to both PPM signal and voltage variables together. In order to do that, different surfaces are fitted to the data sets using Matlab Curve Fitting Toolbox. A similar process was performed in [20] All the surfaces together form the ESC-Motor-Propeller combination mathematical model. This mathematical model will be uploaded on the onboard application later on in order to provide real time performance parameters.

5.1 Thrust vs (PPM and Voltage) Response Surface

Thrust as a function of PPM signal and voltage was fitted to a surface of the form:

$$T(x, v) = p_{00} + p_{10}x + p_{01}v + p_{20}x^2 + p_{11}xv \tag{5.1}$$

where T is the thrust in grams, x is PPM signal in μs and v is the voltage in volts.

Table 5.1: Thrust vs (PPM and Voltage

Item	**Value**
p_{00}	2418
p_{10}	-2.912
p_{01}	-139.1
p_{20}	7.806×10^{-4}
p_{11}	0.1145

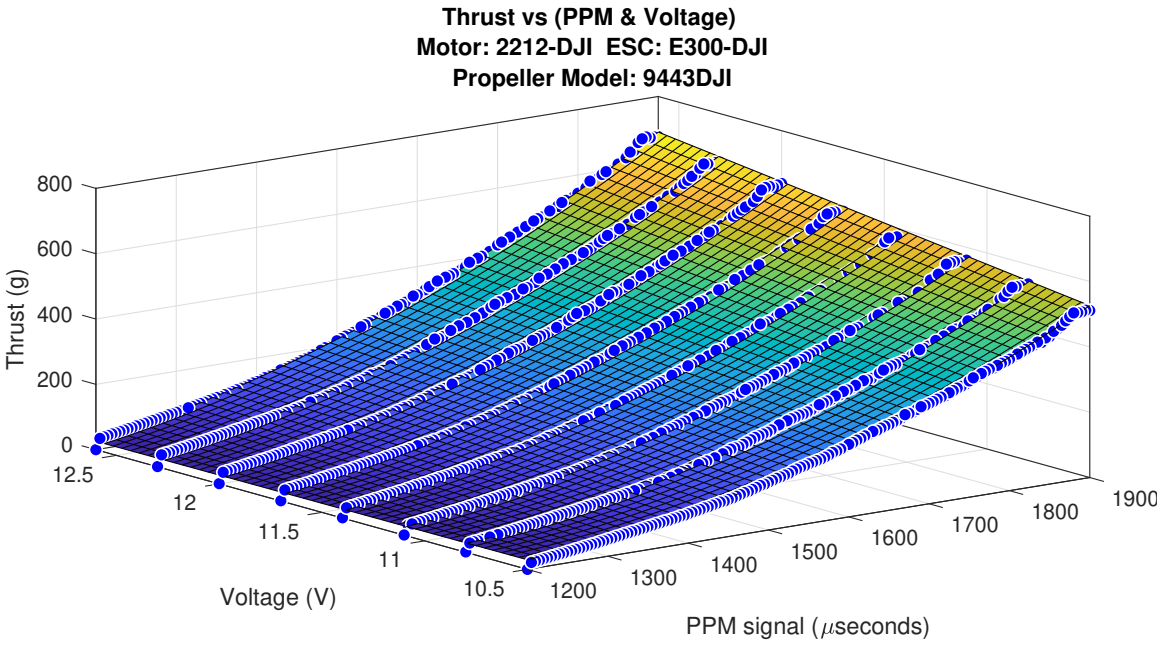

Figure 5.1: Thrust vs (PPM and voltage)

5.2 Current vs (PPM and Voltage) Response Surface

Current as a function of PPM signal and voltage was fitted to a surface of the form:

$$I(x, v) = p_{00} + p_{10}x + p_{01}v + p_{20}x^2 + p_{11}xv + p_{30}x^3 + p_{21}x^2v \tag{5.2}$$

where I is the current in amps, x is PPM signal in μs and v is the voltage in volts.

Table 5.2: Current vs (PPM and Voltage)

Item	**Value**
p_{00}	-51.09
p_{10}	0.09948
p_{01}	3.192
p_{20}	-6.127×10^{-5}
p_{11}	-5.226×10^{-3}
p_{30}	1.149×10^{-8}
p_{21}	2.161×10^{-6}

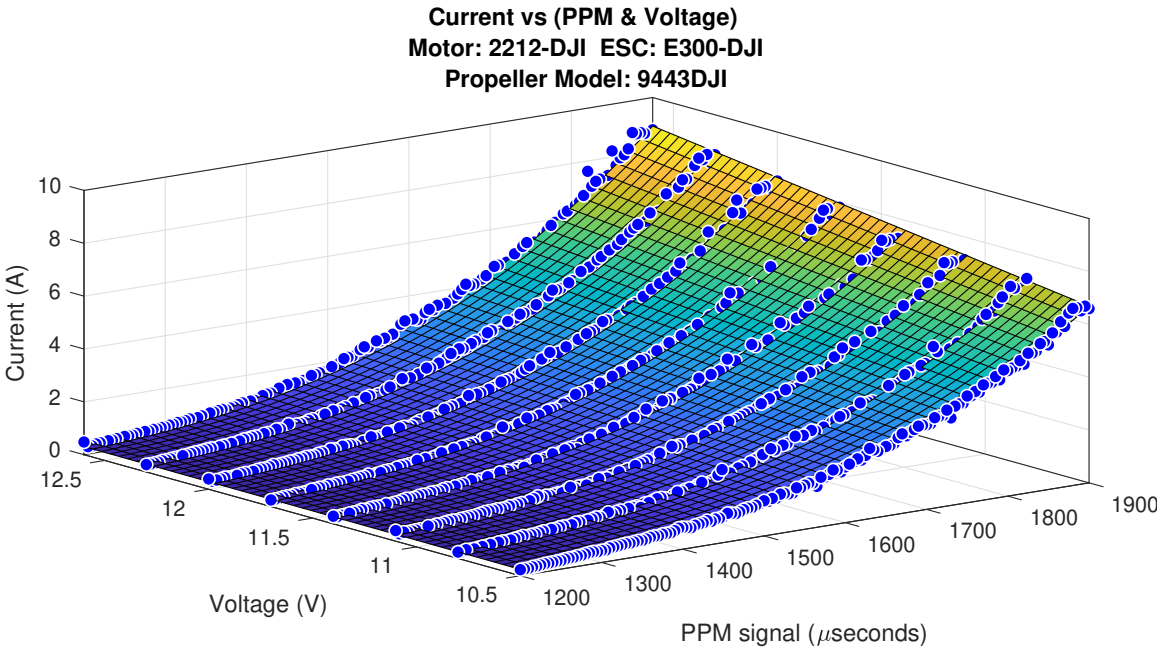

Figure 5.2: Current vs (PPM and voltage)

5.3 Power vs (PPM and Voltage) Response Surface

Power as a function of PPM signal and voltage was fitted to a surface of the form:

$$P(x, v) = p_{00} + p_{10}x + p_{01}v + p_{20}x^2 + p_{11}xv + p_{30}x^3 + p_{21}x^2v \tag{5.3}$$

where P is the power in watts, x is PPM signal in μs and v is the voltage in volts.

Table 5.3: Power vs (PPM and Voltage

Item	**Value**
p_{00}	-876.8
p_{10}	1.591
p_{01}	63.25
p_{20}	-8.729×10^{-4}
p_{11}	-0.102
p_{30}	1.264×10^{-7}
p_{21}	4.162×10^{-5}

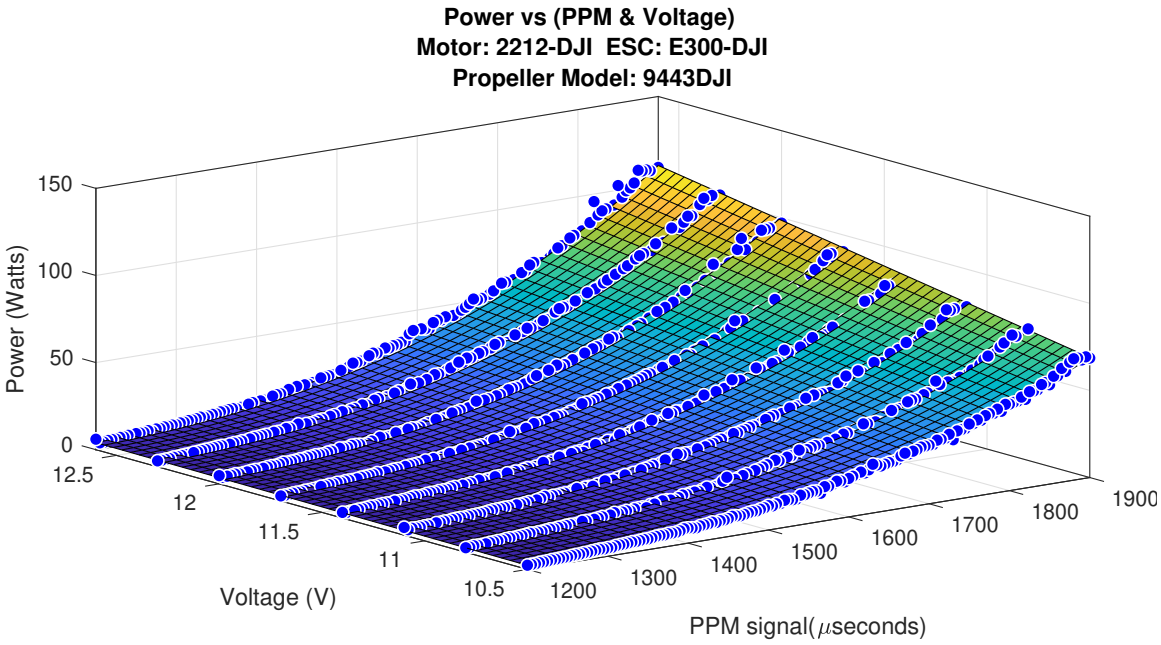

Figure 5.3: Power vs (PPM and voltage)

5.4 Efficiency vs (PPM and Voltage) Response Surface

Efficiency as a function of PPM signal and voltage was fitted to a surface of the form:

$$E(x,v) = p_{00} + p_{10}x + p_{01}v + p_{20}x^2 + p_{11}xv + p_{02}v^2 + p_{30}x^3 + p_{21}x^2v + p_{12}xv^2 + p_{40}x^4 + p_{31}x^3v + p_{22}x^2v^2 + p50x^5 + p41x^4v + p32x^3v^2 \quad (5.4)$$

where E is the efficiency in g/watt, x is PPM signal in μs and v is the voltage in volts.

Table 5.4: Efficiency vs (PPM and Voltage)

Item	Value
p_{00}	-5327
p_{10}	8.831
p_{01}	842.5
p_{20}	-0.004666
p_{11}	-1.379
p_{02}	-271.8
p_{30}	6.128×10^{-7}
p_{21}	7.311×10^{-4}
p_{12}	0.06162
p_{40}	1.215×10^{-10}
p_{31}	-1.118×10^{-7}
p_{22}	-3.458×10^{-5}
p_{50}	-1.593×10^{-14}
p_{41}	-7.093×10^{-12}
p_{32}	6.469×10^{-9}

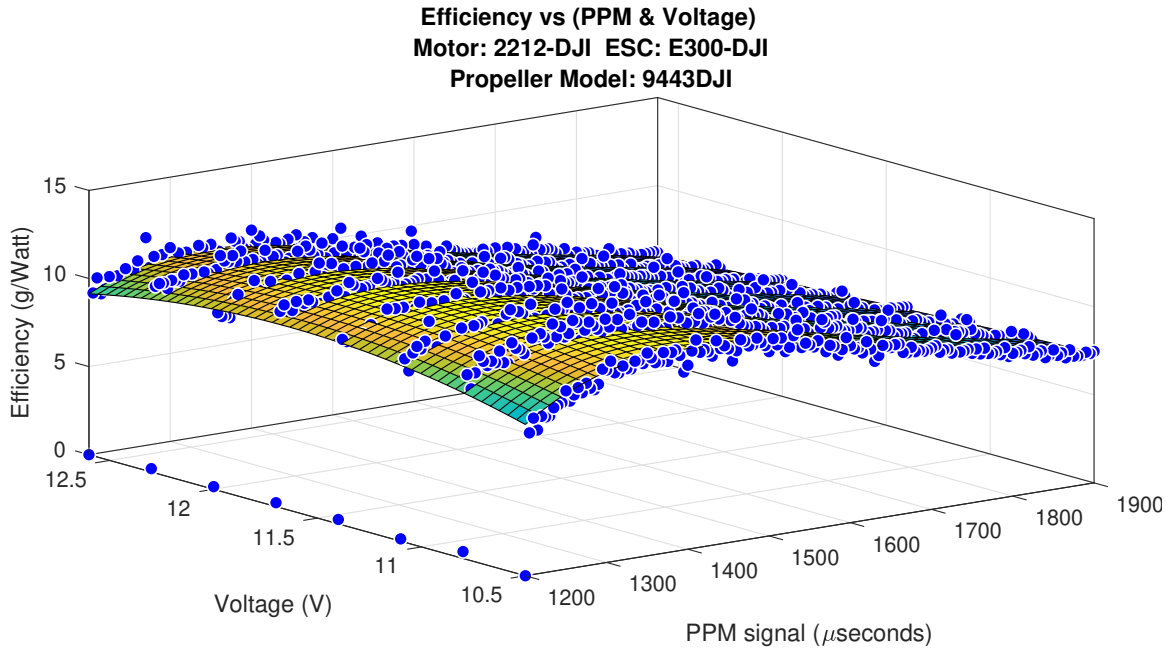

Figure 5.4: Efficiency vs (PPM and voltage)

5.5 RPM vs (PPM and Voltage) Response Surface

RPM as a function of PPM signal and voltage was fitted to a surface of the form:

$$R(x, v) = p_{00} + p_{10}x + p_{01}v + p_{20}x^2 + p_{11}xv \tag{5.5}$$

where R is RPM,x is PPM signal in μs and v is the voltage in volts.

Table 5.5: RPM vs (PPM and Voltage)

Item	**Value**
p_{00}	-3379
p_{10}	2.846
p_{01}	-472.6
p_{20}	-7.33×10^{-5}
p_{11}	0.5398

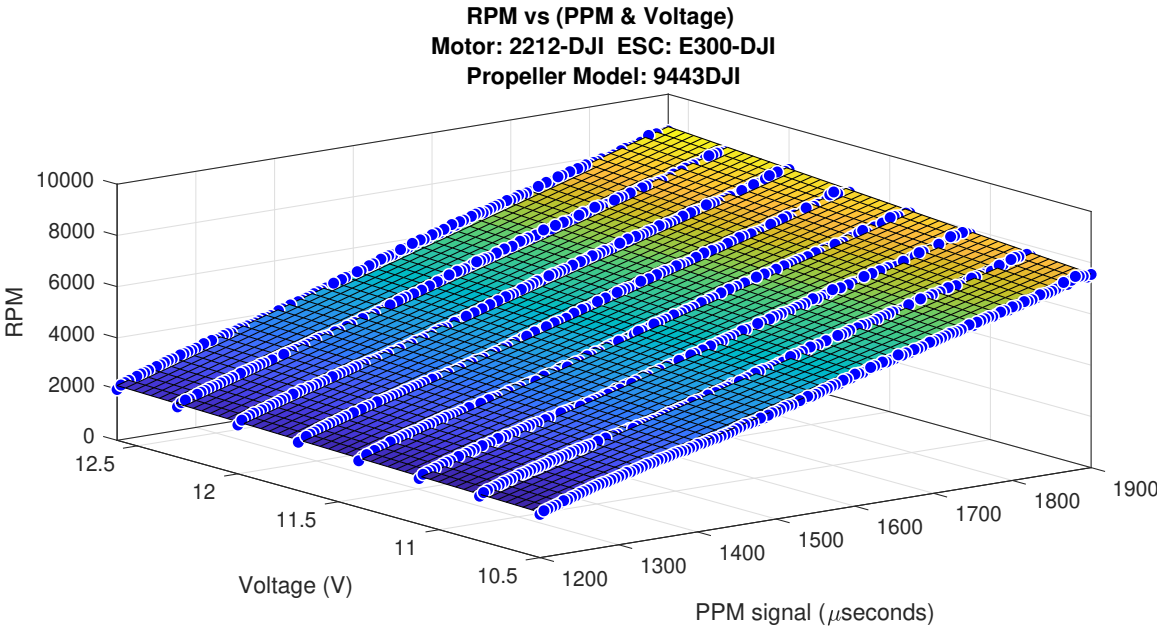

Figure 5.5: RPM vs (PPM and voltage)

CHAPTER 6

ESTIMATION SYSTEM IMPLEMENTATION

In this chapter, once that the ESC-motor-propeller functional relationship is ready, the estimation system will be implemented on the multicopter.

6.1 Estimation System Description

In the previous chapter as a result of different experiments and data processing, an ESC-Motor-Propeller functional relationship model was obtained. This model correlates T, I, P, E and R as a function of battery voltage v and PPM signal x. This performance functional relationship is only valid for the E300-DJI 2212-DJI 9443DJI ESC-Motor-Propeller combination. However, different performance mathematical models for different combinations can be obtained just repeating the experiments described in chapter 4 and following the surface fitting process in chapter 5. During the development of this thesis, a second mathematical model was obtained for the 430LITE-DJI 2312E-DJI 9450DJI combination.

The next step towards the performance parameters estimation is getting from the flight controller the battery voltage values v, and PPM signal x for each one of the motors of the multicopter. After that, these values are plugged in the functional relationship and the performance parameters calculated.

The battery voltage is contained in the ROS topic (mavros/battery), and the PPM signal in each one of the motors are contained in the ROS topic (mavros/rc/out). In order to read the topics from the Pixhawk 4 mini flight controller the estimation systems uses MAVROS. This extendable communication node for Robot Operating

System (ROS) was installed in an onboard Raspberry Pi 3+. This onboard computer running ROS, performs the calculations. The Raspberry Pi 3+ is accessed remotely via Putty, a SSH and telnet client. Finally the estimated performance parameters displayed in the ground station (laptop). A scheme of how the estimation system is implemented is shown in figure 6.1

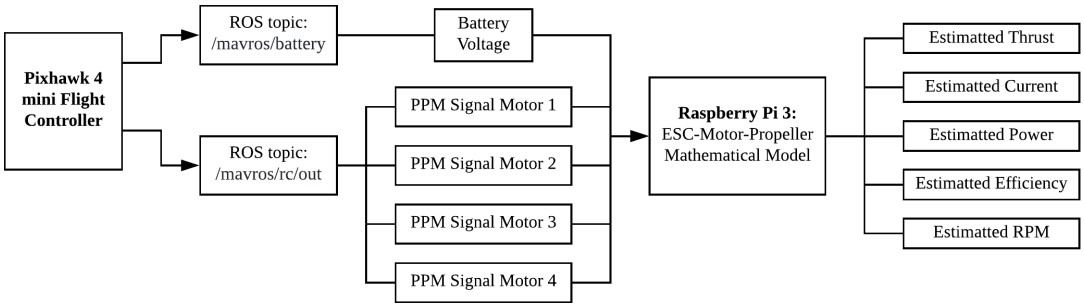

Figure 6.1: Estimation system scheme

6.2 Results Validation

For the validation of the Estimation System, different experiments were performed in order to set against the estimated values and the actual ones and calculate the error.

6.2.1 Estimated Thrust Validation

The experiment performed to validate the estimated weight consists in a series of hovering stationary flights. In each flight the multicopter took off with or without payload, powered by different sized batteries. Then the multicopter was made to fly in hovering stationary conditions using hold flight mode. This flight mode keeps the multicopter fixed at determined altitude and position using GPS and barometer

sensors. Once the multicopter is hovering stabilized, at a fixed altitude and position, the lecture of the estimated thrust was read.

Different object combinations were used as payload. The weight of these objects was measured using a scale, the values are shown in table 6.1.

Table 6.1: Table of weights

Item	**Weight (g)**
Empty 450 Quadcopter	984
4000 mAh LiPo Battery	331
5000 mAh LiPo Battery	396
5000 mAh NiMH Battery	427
280 Quadcopter	294

A series of seven experiments were performed. The multirotor flew with different combinations of batteries and external payloads. Different objects where lifted using a cable to create different payload scenarios. After the experiments, the estimated and actual values where compared and the error calculated:

First, the quadcopter flew powered by a 4000 mAh LiPo battery, the empty quadcopter weight was estimated five times and averaged, the results are shown in table 6.2

Table 6.2: Empty weight estimation powered by a 4000 mAh LiPo battery

Measured Empty Weight (g)	1315

Experiment	**Estimated Empty Weight (g)**	**% Error**
1	1284.18	2.34
2	1270.35	3.40
3	1292.58	1.70
4	1274.03	3.12
5	1270.18	4.20
Average	1298.26	1.27

Then a payload of 294 g was attached. The estimated payload weight was calculated using equation 6.1.

$$EstimatedPayloadWeight = EstimatedTotalWeight - EstimatedEmptyWeight \tag{6.1}$$

The experiment was repeated five times and averaged. The results are shown in table 6.3

Table 6.3: 294 g payload weight estimation powered by a 4000 mAh LiPo battery

Estimated Empty W(g)	1298.26
Measured Payload W (g)	294
Measured Total W (g)	1609

Exp	**Estimated Total W (g)**	**% Error**	**Estimated Payload W (g)**	**% Error**
1	1650.00	2.55	351.74	19.64
2	1565.99	2.67	267.73	8.94
3	1678.86	4.34	380.60	29.45
4	1548.32	3.77	250.06	14.95
5	1608.85	0.01	310.59	5.64
Avg	1610.40	0.09	312.14	6.17

The same process was made for a payload of 396 g. The results are shown ion table 6.4

Table 6.4: 396 g payload weight estimation powered by a 4000 mAh LiPo battery

Estimated Empty W (g)	1298.26
Measured Payload W (g)	396
Measured Total W (g)	1711

Exp	**Estimated Total W (g)**	**% Error**	**Estimated Payload W(g)**	**% Error**
1	1749.00	2.22	450.74	18.62
2	1652.58	3.41	354.32	14.18
3	1617.64	5.46	319.38	26.06
4	1719.69	0.51	421.43	8.65
5	1689.21	1.27	390.95	1.75
Avg	1685.62	1.48	387.36	2.18

Then the internal battery was replaced by a 5000 mAh LiPo battery, in the same way, the empty weight was calculated again. the results are shown in table 6.5

Table 6.5: Empty weight estimation powered by a 5000 mAh LiPo battery

Measured Empty Weight (g)	1380

Experiment	**Estimated Empty Weight (g)**	**% Error**
1	1361.17	1.36
2	1430.65	8.79
3	1333.77	1.43
4	1364.34	3.75
5	1353.72	2.94
Average	1368.73	4.09

Then the payload weight estimation experiments where repeated for different payloads. The results are shown in tables 6.6, 6.7, 6.8 and 6.9

Table 6.6: 396 g payload weight estimation powered by a 5000 mAh LiPo battery

Estimated Empty W (g)	1368.73
Measured Payload W (g)	396
Measured Total W (g)	1776

Exp	**Estimated Total W (g)**	**% Error**	**Estimated Payload W (g)**	**% Error**
1	1785.00	0.51	416.27	5.12
2	1741.99	1.91	373.26	5.74
3	1753.3	1.28	384.57	2.89
4	1792.67	0.94	423.94	7.06
5	1772.99	0.17	404.26	2.09
Avg	1769.19	0.38	400.46	1.13

Table 6.7: 427 g payload weight estimation powered by a 5000 mAh LiPo battery

Estimated Empty W (g)	1368.73
Measured Payload W (g)	427
Measured Total W (g)	1807

Exp	**Estimated Total W (g)**	**% Error**	**Estimated Payload W (g)**	**% Error**
1	1810.00	0.17	441.27	3.34
2	1747.57	3.29	378.84	11.28
3	1769.12	2.09	400.44	6.22
4	1828.96	1.22	460.23	7.78
5	1700	5.92	331.27	22.42
Avg	1771.14	1.98	402.41	5.76

Table 6.8: 690 g payload weight estimation powered by a 5000 mAh LiPo battery

Estimated Empty W (g)	1368.73
Measured Payload W (g)	690
Measured Total W (g)	2070

Exp	**Estimated Total W (g)**	**% Error**	**Estimated Payload W (g)**	**% Error**
1	2075.00	0.24	706.27	2.36
2	1993.89	3.68	625.16	9.40
3	2064.63	0.26	695.90	0.86
4	2096.28	1.27	727.55	5.44
5	2057.12	0.62	688.39	0.23
Avg	2057.38	0.61	688.65	0.20

Table 6.9: 721 g payload weight estimation powered by a 5000 mAh LiPo battery

Estimated Empty W (g)	1368.73
Measured Payload W (g)	721
Measured Total W (g)	2101

Exp	**Estimated Total W (g)**	**% Error**	**Estimated Payload W (g)**	**% Error**
1	2117.00	0.76	748.27	3.78
2	2017.41	3.98	648.68	10.03
3	2055.01	2.19	686.28	4.82
4	2112.96	0.57	744.23	3.22
5	2082.18	0.90	713.45	1.05
Avg	2076.91	1.15	708.18	1.78

6.2.2 Estimated Current, Power and RPM Validation

The experiment that validated the estimated Current, Power and RPM was simple. The multicopter was armed and the throttle input signal was increased making the motors spin faster. Values of the estimated current, power and RPM were taken. The estimated and real values where compared

- Estimated current and power are compared with the values provided by the Pixhawk onboard sensors
- Estimated RPM was compared with the real values measured with a laser tachometer

The experiment was repeated five times, the results are shown in tables 6.10, 6.11 and 6.12

Table 6.10: Estimated and real current in Amps

Exp	**Real**	**Estimated**	**% Error**
1	2.12	1.39	8.96
2	2.86	2.84	0.70
3	5.78	5.7	1.38
4	8.81	8.78	0.34
5	24.4	24.49	0.37

Table 6.11: Estimated and real power in Watts

Exp	**Real**	**Estimated**	**% Error**
1	23.2	21.2	8.62
2	31.22	30.73	1.57
3	63.8	61.8	3.13
4	75.51	78.57	4.05
5	272.57	273.54	0.36

Table 6.12: Estimated and real RPM

Exp	**Real**	**Estimated**	**% Error**
1	2120	2100	0.92
2	2096	2083	0.62
3	3574	3365	5.85
4	5077	5171	1.85
5	7567	7407	2.11

CHAPTER 7

PERFORMANCE COMPARISON

In this chapter, the results of testing two ESC-Motor combinations with different propeller models are shown and compared. The objective of this study is to compare the effect of the propeller on the performance of the combination and compare the two ESC-Motor combinations between them. These experiments make possible to study how the variations of the propeller diameter, pitch and number of blades influence its performance. This information is very useful to select the perfect combination for an specific multicopter or mission.

Five different propeller models where tested: 9443DJI, 9450JI, 9443DJI Triblade, 1045DJI and 1045 Gemfan. Unfortunately, the last model could not be attached to the 2312E motor. The experiments were conducted at contsant 12.6 volts and variable PPM signal. E300 and 430LITE ESCs are operating in a different PPM signal range. The E300-2212 combination was tested for PPM signal values from 1200 to 1900 μs. The 430LITE-2312E combination was tested for PPM signal values from 1200 to 1800 μs.

7.1 Thrust vs PPM Signal

As shown in figures 7.1 and 7.2, and table 7.1, the maximum thrust produced by the E300-2212 combination is slightly superior. Also can be noticed that the thrust vs PPM signal response is different depending on the propeller model, motor and ESC combination.

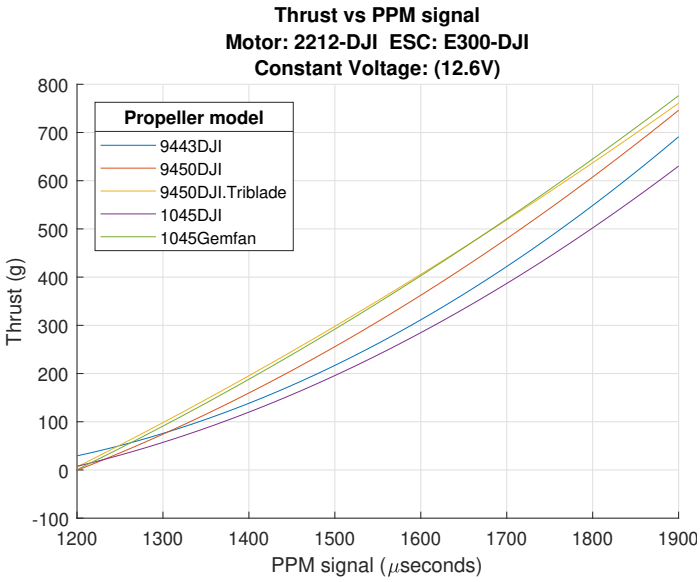

Figure 7.1: 2212-DJI motor thrust vs PPM

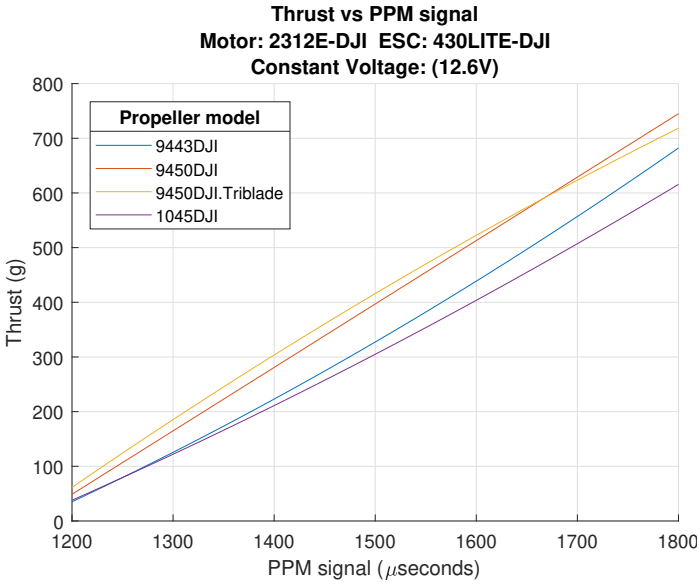

Figure 7.2: 2312E-DJI motor thrust vs PPM

Table 7.1: Maximum thrust in grams

ESC-Motor	9444 DJI	9450 DJI	9450 DJI-Tri	1045 DJI	1045 Gemfan
E300-2212	681.85	730.45	743.69	615.94	754
430LITE-2312E	681	734.11	708	607	none

7.2 Current vs PPM Signal

As shown in figures 7.3 and 7.4, and table 7.2, the maximum current drawn is higher for the E300-2212 combination. Can be also noticed that the propellers that produced a higher thrust drawn more current.

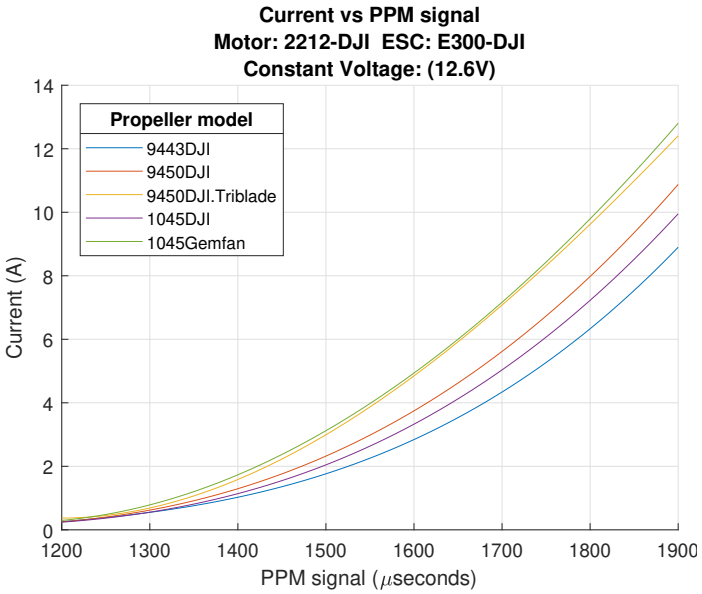

Figure 7.3: 2212-DJI motor current vs PPM

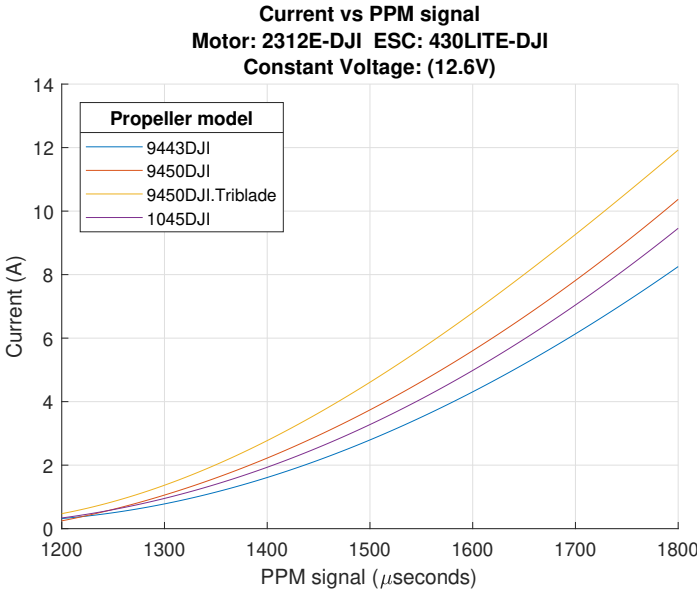

Figure 7.4: 2312E-DJI motor current vs PPM

Table 7.2: Maximum current in amps

textbfESC-Motor	**9444 DJI**	**9450 DJI**	**9450 DJI-Tri**	**1045 DJI**	**1045 Gemfan**
E300-2212	8.89	10.87	12.40	9.95	12.80
430LITE-2312E	8.25	10.35	11.93	9.46	none

7.3 Power vs PPM Current

The same happens with the power, as shown in figures 7.5 and 7.6, and table 7.3 since $P = VI$ and the voltage is a constant.

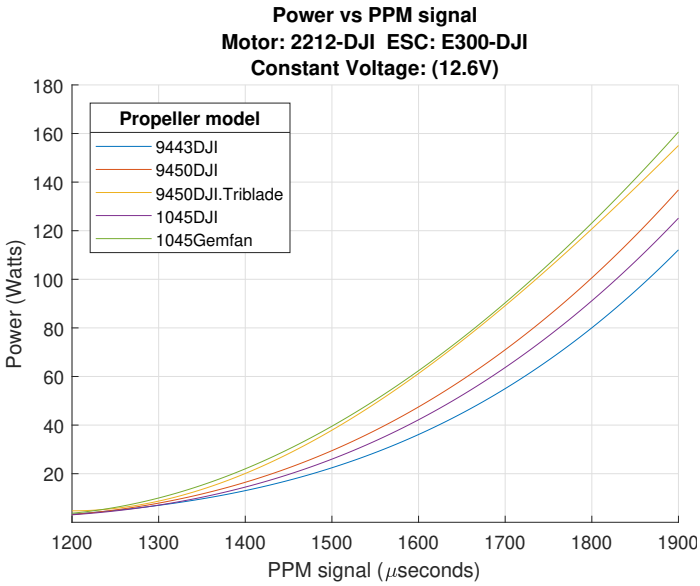

Figure 7.5: 2212-DJI motor power vs PPM

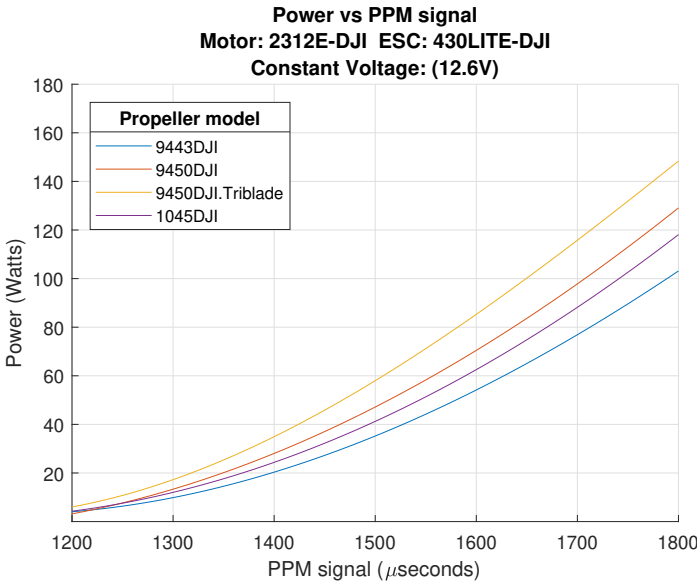

Figure 7.6: 2312E-DJI motor power vs PPM

Table 7.3: Maximum power in watts

ESC-Motor	9444 DJI	9450 DJI	9450 DJI-Tri	1045 DJI	1045 Gemfan
E300-2212	112.12	136.80	155.06	125.18	160.64
430LITE-2312E	103.14	129.09	148.36	118.09	none

7.4 Efficiency vs PPM Signal

In the case of the efficiency, in figures 7.7 and 7.8 it is shown that every combinations presents a totally different pattern:

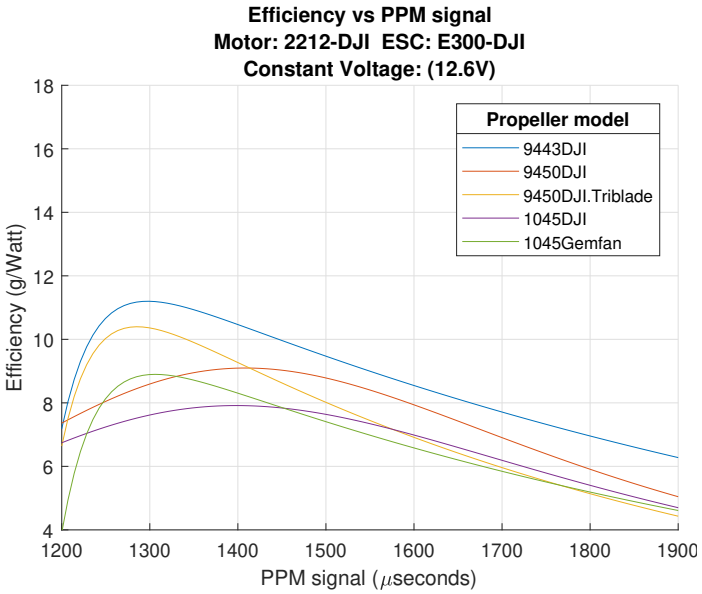

Figure 7.7: 2212-DJI motor efficiency vs PPM

In table 7.4 the maximum values of the efficiency curve for the E300-2212 are displayed.

Table 7.4: Maximum efficiency points in g/watt

ESC-Motor	9444 DJI	9450 DJI	9450 DJI-Tri	1045 DJI	1045 Gemfan
E300-2212	11.48	10.55	11.81	9.09	9.15

The 430LITE-2321 combination does not present these maximum efficiency points

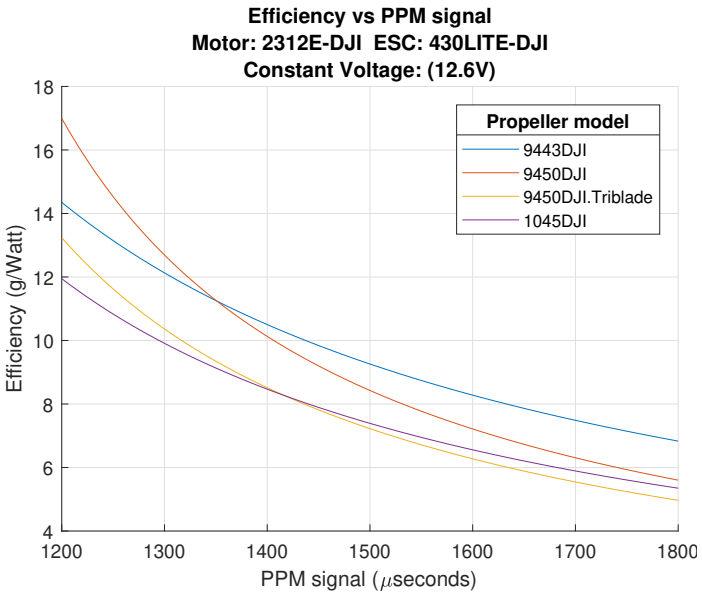

Figure 7.8: 2312E-DJI motor efficiency vs PPM

As shown in table 7.5, the 430LITE-2312E combination is more efficient.

Table 7.5: Maximum efficiency at maximum power in g/watt

ESC-Motor	9444 DJI	9450 DJI	9450 DJI-Tri	1045 DJI	1045 Gemfan
E300-2212	6.28	5.04	4.43	4.70	4.61
430LITE-2312E	6.83	5.60	4.97	5.35	none

7.5 RPM vs PPM Signal

The increase of the propeller pitch, diameter and number of blades produces a decrease in the RPM. As shown in figures 7.9 and 7.10, and table 7.6

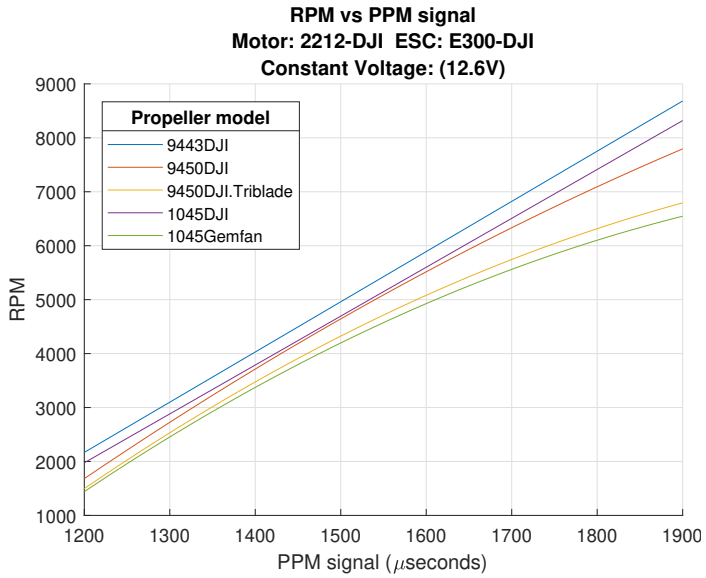

Figure 7.9: 2212-DJI motor RPM vs PPM

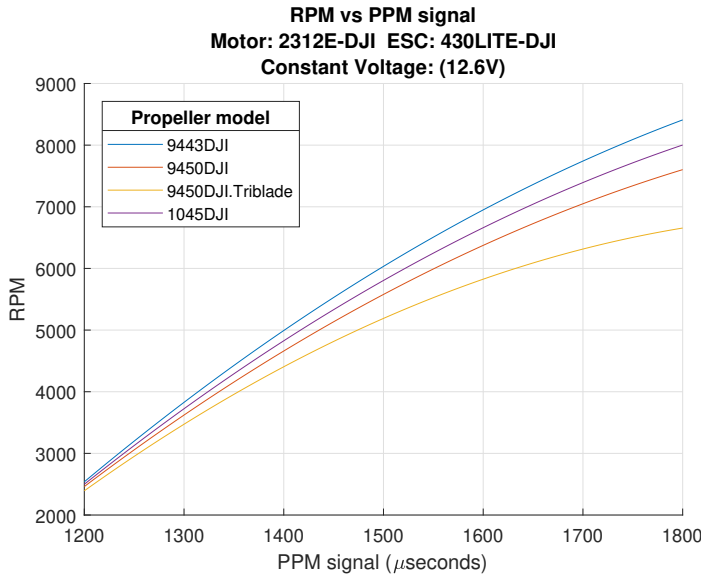

Figure 7.10: 2312E-DJI motor RPM vs PPM

In table 7.6, can be noticed that RPM are slightly higher for E300-2212 combination. The reason is that 2212 motor is 920KV and 2312E motor is 800KV. KV is

defined as the RPM that a motor turns when 1 volt is applied with no load attached to it.

Table 7.6: Maximum RPM

ESC-Motor	9444 DJI	9450 DJI	9450 DJI-Tri	1045 DJI	1045 Gemfan
E300-2212	8682	7794	6794	8319	6547
430LITE-2312E	8409	7602	6655	8002	none

7.6 Temperature vs PPM Signal

Finally in figures 7.11 and 7.13, and table 7.7 can be observed that the propellers with higher power consumption tend to produce higher overheat of the motor. The 430LITE-2312E combination finished the experiments with higher temperatures.

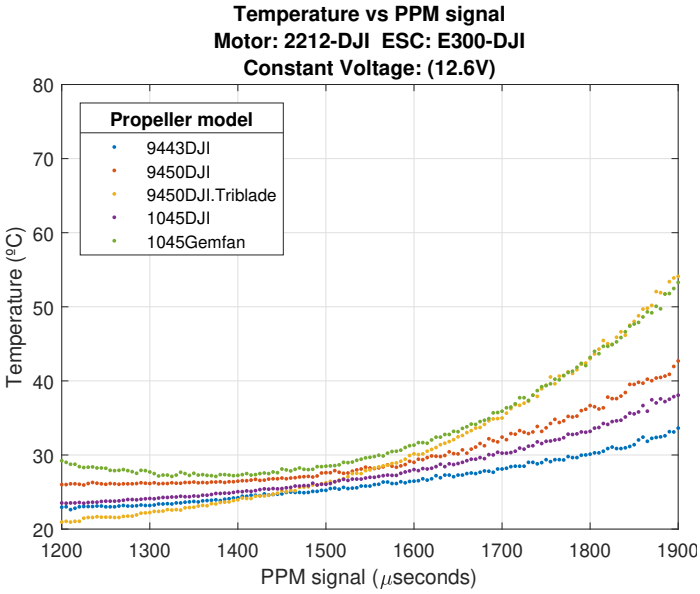

Figure 7.11: 2212-DJI motor temperature vs PPM

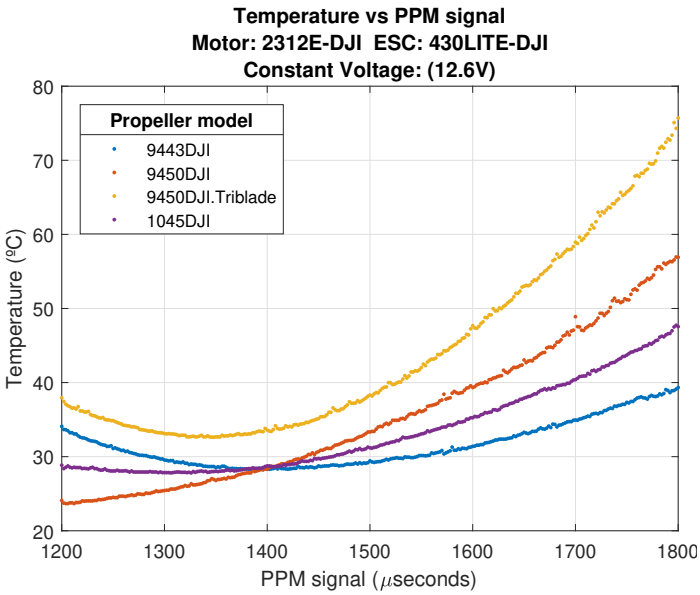

Figure 7.12: 2312E-DJI motor temperature vs PPM

Table 7.7: Maximum temperature in ^{o}C

ESC-Motor	9444 DJI	9450 DJI	9450 DJI-Tri	1045 DJI	1045 Gemfan
E300-2212	33.63	42.69	54.11	38.07	53.29
430LITE-2312E	39.33	56.95	47.73	75.71	none

CHAPTER 8

CONCLUDING REMARKS AND FUTURE WORK

8.1 Thesis Contribution

An estimation system that could be implemented in multicopters with cable suspended payloads without using extra sensors is presented in this thesis. Finally the estimation system was able not only to estimate the weight but also thrust, current, power, efficiency and RPM. The major focus of the work was on

- Developing of formulation for the estimation system
- Designing and building a test bench
- Obtaining a functional representation of the electric propulsion performance parameters
- Performance comparison of two different ESC-Motor combination with different propellers

The functional relationship that correlates PPM signal x and the battery voltage v with T, I, P, E and R obtained empirically and is unique for each ESC-Motor-Propeller combination. The onboard implementation was achieved using ROS.

8.2 Future Work

The work presented gives a foundation to the feasibility of the implementation of the estimation system. Some future studies that can be done are,

- Framework extension for dynamic estimation of the moment of inertia matrix using the total mass, the applied force/moment measurements, and the gyro (angular velocity) outputs

- Study of a physics based model for additional scaling
- Enhance the test bench by adding a torque meter, vibration sensor and acoustic measurements

8.3 Final Words

The work presented in this thesis shows that this estimation system works and can play a crucial role in the future of the aerial transportation using multicopters. The application of this system to multicopters would be ideal to give estimation of weight, thrust, current, power, efficiency and RPM without any aditional sensors.

APPENDIX A

TEST BENCH DESIGN

A.1 Test Bench Parts

These are the components of the test bench explained in detail.

A.1.1 Micro-controller

The brain of the test bench is the Arduino compatible Osepp uno r3 plus micro-controller. This board has the same appearance and features than Arduino UNO. This board uses the 8-bit, AVR, RISC-based ATmega328P micro-controller from Atmel. ATmega328P comes with the Arduino bootloader preloaded. Compatible with existing Arduino software libraries and uses the same Arduino programming console (IDE). The programming language is C++. There are some differences from the original Arduino UNO. Replaced USB-B connector with more popular mini-USB connector. Added Molex connector for easy connect to OSEPP™ sensors and other I2C devices.

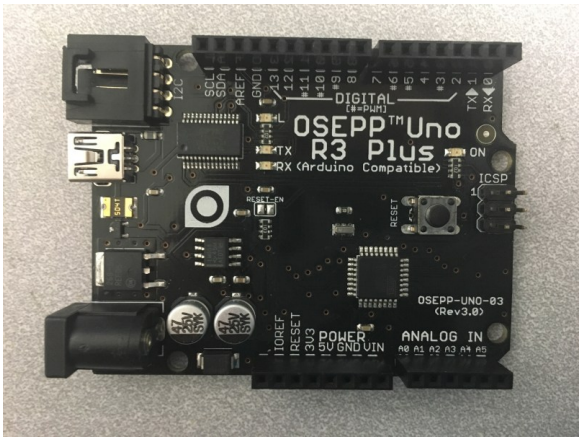

Figure A.1: Osepp UNO r3 plus board

A.1.2 3D Printed Stand

Using SolidWorks the author designed and built a stand that works as a support. The motor, load cell and some sensors are mounted on the stand. The stand if fixed

by screws to the base,that is a piece of wood. All the pieces of this stand were 3D printed at UTA Fablab.

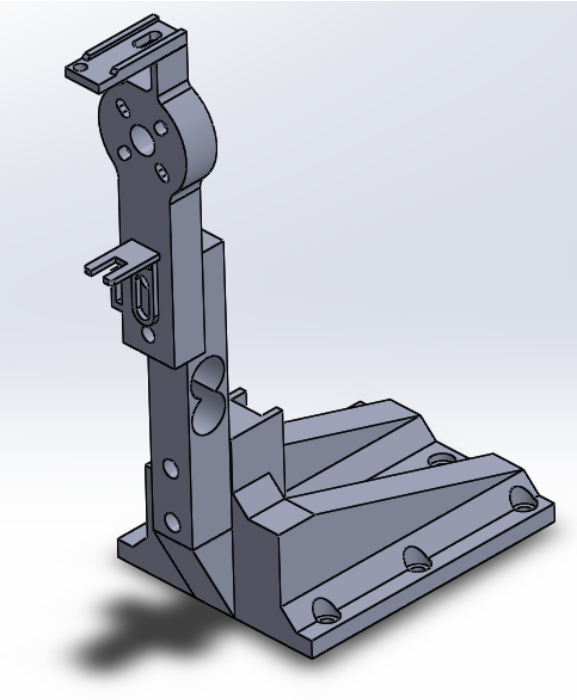

Figure A.2: 3D printed stand

A.1.3 Electronic Speed Controller

ESC stands for Electronic Speed Controller, and it is the electronic circuit that drives a brushless motor. It receives PPM signal form the micro-controller to vary motor's speed, its direction and possibly also to act as a dynamic brake.

Figure A.3: DJI E300 Opto ESC
(Image Courtesy:
www.bhphotovideo.com)

A.1.4 DC Brushless Motor

DC brushless motors are extensively used for multicopters propulsion systems. These type of DC motors are way more powerful for their weight than brushed motors, and they last way longer. Efficiency wise, brushless motors are typically more efficient than brushed motors. This DC motors require an ESC.

Figure A.4: DJI 2212 920KV
(Image Courtesy:
www.hobbyking.com)

A.1.5 Load Cell and HX711 Amplifier

A load cell is a transducer which converts force into a measurable electrical output. There are many varieties of load cells, a Bending beam load cell was chosen. That kind of devices are made of aluminum alloy, have a capacity range from 1 to 500 Kg and are cost efficient. The load cell installed on the test bench is a model with a range capacity of 5 Kg, more than enough for the common sized brushless motors.

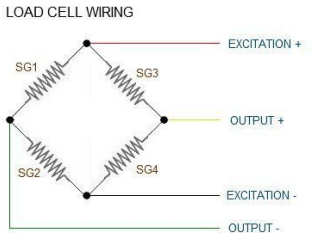

Figure A.5: Load Cell scheme (Image Courtesy: learn.sparkfun.com)

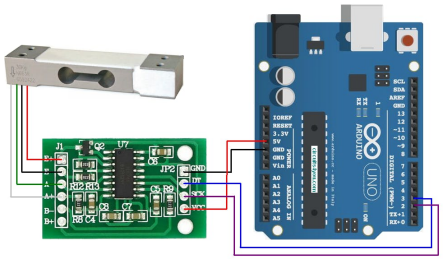

Figure A.6: HX11 and Load Cell scheme (Image Courtesy: www.hackster.io)

HX711 is a precision 24-bit analog-to-digital converter (ADC) designed for weigh scales. All controls to the HX711 are through pins. The input can be done through either Channel A or B. Channel A can be programmed with a gain of 128 or 64, corresponding to a full-scale differential input voltage of ±20 mV or ±40 mV respectively, when a 5 V supply is connected to AVDD analog power supply pin. Channel B has a fixed gain of 32. I used channel A to connect the load cell.

A.1.6 ACS712 Current Sensor

ACS712 Current Sensors are designed to be easily used with Arduino compatible micro-controllers. These sensors are based on the Allegro ACS712ELC chip and

are offered with full scale values of 5 A, 20 A and 30 A. The sensors are bi-directional, which means that can measure current in both directions. The DJI E300 Opto ESC is rated for currents of maximum 15 A, but to have margin for future more powerful ESC´s, the 30 A model was chosen. The sensor was supposed to come factory calibrated and the offset and slope provided. However, the received sensor was not following this parameters and they had to be experimentally determined.

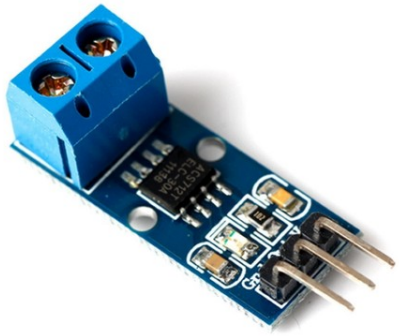

Figure A.7: ACS712 Current Sensor
(Image Courtesy:
crelectrons.com)

A.1.7 B25 Voltage Sensor

A simple, inexpensive and very useful module which uses a potential divider to reduce any input voltage by a factor of 5. Using one of the analog inputs of the micro-controller to monitor voltages up to 25 V. This sensor did not need calibration and was really straight forward.

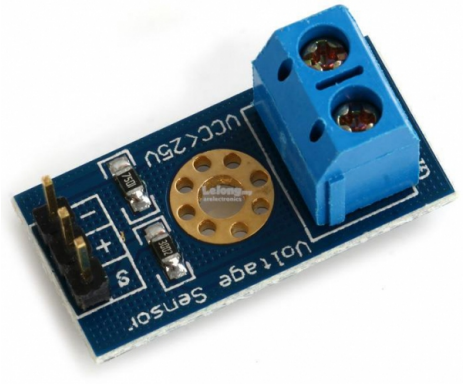

Figure A.8: B25 Voltage Sensor
(Image Courtesy:
www.geeker.co.nz)

A.1.8 Optic Infra Red RPM Sensor

A RPM sensor was designed and built in order to track the motor rotational speed. The IR sensor was built using a TCRT5000 module, some resistors and wires. TCRT5000 is a reflective sensor which includes an IR led and an IR photo-transistor in a leaded package which blocks visible light. The sensor basically opens the circuit when detects IR light and closes it if not.

Figure A.9: TCRT5000 Reflective Sensor
(Image Courtesy:
www.fabtolab.com)

A.1.9 MLX90615 Infra Red Temperature Sensor

This sensor was added to the test bench in order to control if there is motor overheat. If the propeller were too heavy for the motor (the motor would not have enough torque to drive it) it would result in a motor malfunction and overheating. Theretofore, the motor temperature has to be measured during the tests to detect if a propeller is not adequate for an specific brushless motor.

The MLX90615 is a miniature infrared thermometer for non-contact temperature measurements. The sensor can provide the object temperature and the ambient temperature as well. With this feature, I will have in my records the ambient temperatures in the moment of the tests.

The sensor is factory calibrated in wide temperature range: -20 to 85°C for sensor temperature and -40 to 115 °C for object temperature, with a measurement resolution of 0.02 °C

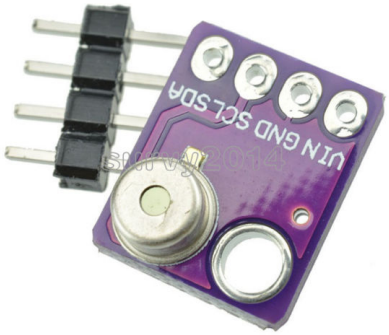

Figure A.10: MLX90615 IR Temperature Sensor
(Image Courtesy:
www.ebay.com)

A.1.10 Batteries

For some tests, LiPo (Lithium polymer) batteries were used. Lithium polymer batteries are composed of cells. Each cell is considered to be fully charged at 4.20 V, and discharged at 3.5 V. In this case, a three cells battery is fully charged when voltage is 12.60 and discharged when it reaches 10.50 V. The batteries are the same ones that are used on the quadcopter: Turnigy 3S 11.4 V 4000 mAh 20-30C discharge.

Figure A.11: Turnigy 3S 11V 4000mAh batteries

A.1.11 Variable Voltage Power Source

Since batteries are fluctuating from 12.60 V to 10.50 V, for some tests was necessary the use of a power source that could provide current at constant voltage. A lab grade regulated voltage power source had to be acquired. The specific model was TekPower TP1540E DC 30V 20A. It can provide current within a range of 0-30 V with a maximum of 20 A, or within 0-20 A with a maximum of 30 V.

Figure A.12: TekPower TP1540E DC 30V 20A power supply

A.2 Test Bench Wiring Diagram

In figure a wiring diagram of the test bench and all its sensors and components is shown in fig A13:

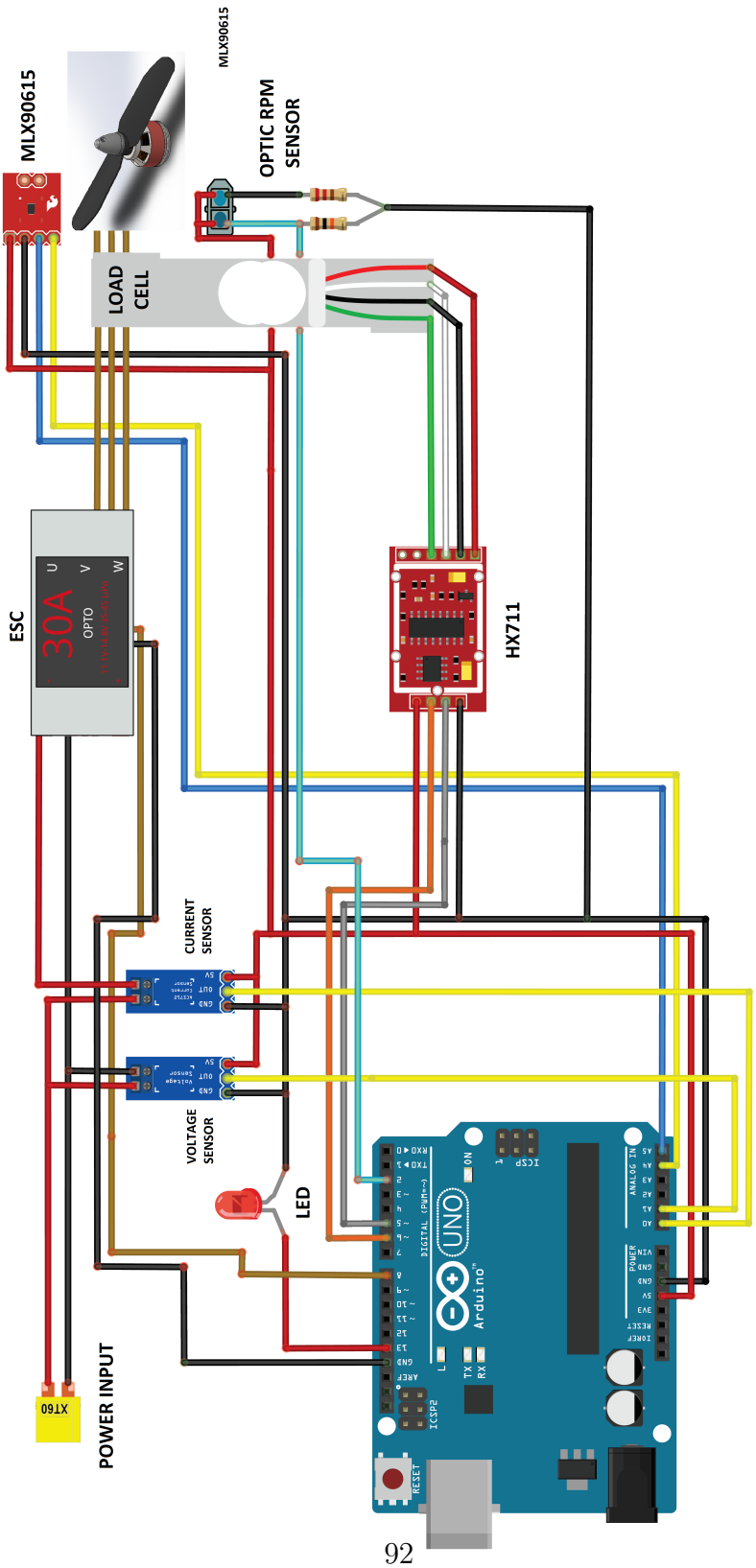

Figure A.13: Test bench wiring diagram

REFERENCES

[1] M. Bartholmai and P. Neumann, "Micro-drone for gas measurement in hazardous scenarios via remote sensing," in *Proceedings of*, 2010.

[2] K. Turkoglu and A. ji, "Development of a low-cost experimental quadcopter testbed using an arduino controller for video surveillance," 01 2015.

[3] E. Natalizio, R. Surace, V. Loscri, F. Guerriero, and T. Melodia, "Filming Sport Events with Mobile Camera Drones: Mathematical Modeling and Algorithms," research report, Dec. 2012.

[4] H. Saha, S. Basu, S. Auddy, R. Dey, A. Nandy, D. Pal, N. Roy, S. Jasu, A. Saha, S. Chattopadhyay, and T. Maity, "A low cost fully autonomous gps (global positioning system) based quad copter for disaster management," in *2018 IEEE 8th Annual Computing and Communication Workshop and Conference (CCWC)*, pp. 654–660, Jan 2018.

[5] Z. Bassett, M. Holdren, D. Vutetakis, A. Bass, P. Finch, A. Flock, M. Darrow, H. Kwan, and D. Tansel, *An Unmanned VTOL and Fixed Wing Vehicle Equipped for Package Retrieval and Delivery.*

[6] J. T. Zou, Z. Y. Pan, D. L. Zhang, and R. F. Zheng, "Integration of the target position correction software with the high endurance quadcopter for search and rescue mission," in *Modern Design Technologies and Experiment for Advanced Manufacture and Industry*, vol. 764 of *Applied Mechanics and Materials*, pp. 713–717, Trans Tech Publications, 6 2015.

[7] D. Bamburry, "Drones: Designed for product delivery," *Design Management Review*, vol. 26, no. 1, pp. 40–48.

[8] R. W. Bulaga and J. N. Portlock, *FlyKart - Mini Personal Air Vehicle*.

[9] D. Mellinger, Q. Lindsey, M. Shomin, and V. Kumar, "Design, modeling, estimation and control for aerial grasping and manipulation," in *2011 IEEE/RSJ International Conference on Intelligent Robots and Systems*, pp. 2668–2673, Sep. 2011.

[10] P. Martin and E. Salaün, "The true role of accelerometer feedback in quadrotor control," in *2010 IEEE International Conference on Robotics and Automation*, pp. 1623–1629, May 2010.

[11] R. C. Leishman, J. C. Macdonald, R. W. Beard, and T. W. McLain, "Quadrotors and accelerometers: State estimation with an improved dynamic model," *IEEE Control Systems Magazine*, vol. 34, pp. 28–41, Feb 2014.

[12] , "VICON." `https://www.vicon.com/`. [Online; accessed 4-May-2019].

[13] D. Ho, J. Linder, G. Hendeby, and M. Enqvist, "Mass estimation of a quadcopter using imu data," in *2017 International Conference on Unmanned Aircraft Systems (ICUAS)*, pp. 1260–1266, IEEE, 2017.

[14] J. Bazin, T. Fields, and A. J. Smith, *Feasibility of In-Flight Quadrotor Individual Motor Thrust Measurements*.

[15] H. Das, V. Baskaran, and H. Arya, "Static performance analysis of electric propulsion system in quadrotors," in *2016 International Conference on Control, Instrumentation, Communication and Computational Technologies (ICCICCT)*, pp. 495–500, Dec 2016.

[16] C. E. Tinney and J. Sirohi, "Multirotor drone noise at static thrust," *AIAA Journal*, vol. 56, no. 7, pp. 2816–2826, 2018.

[17] C. Wisniewski, A. Byerley, K. W. V. Treuren, and A. Hays, *A Comparison of the Aerodynamic Performance and Aeroacoustic Behavior of Commercial and Custom Designed Quadcopter Propellers*.

[18] , "ARDUINO." https://www.arduino.cc//. [Online; accessed 2-May-2019].

[19] MathWorks, "MATLAB." https://www.mathworks.com/products/matlab.html. [Online; accessed 1-May-2019].

[20] G. Szafranski, R. Czyba, and M. BŁachuta, "Modeling and identification of electric propulsion system for multirotor unmanned aerial vehicle design," in *2014 International Conference on Unmanned Aircraft Systems (ICUAS)*, pp. 470–476, May 2014.

[21] , "Robotic Operating System ROS." https://www.ros.org/about-ros/. [Online; accessed 1-May-2019].

BIOGRAPHICAL STATEMENT

Abel Martinez Martinez was born in Murcia, Spain, in 1990. He received his B.E. degree from Universidad Politecnica de Cartagena (UPCT), Spain, in 2014, in Naval Engineering. While pursuing this B.E. he was a cadet Commissioned Officer of Spanish Air Force, in the Spanish Air force Academy, Murcia, from 2010-2011. Few years later, he received his second B.E. degree from Universidad Miguel Hernandez de Elche (UMH), Spain, in 2015, in Mechanical Engineering. During the last year of his B.E. degree in Mechanical Engineering was taken during an ERASMUS exchange program of two semesters in Akademia Górniczo-Hutnicza im. Stanisława Staszica w Krakowie (AGH University of Science and Technology), Poland, in 2015. After his graduation he stayed in Poland from until 2016 as an intern in Valeo Autosistemy SP. Z.O.O. Thermal System Skawina (Poland), his role was Validation Plan Following, CAD following, support for Project Fan System Development.

He joined the University of Texas at Arlington in Summer 2017 to pursue an M.S. program in Aerospace Engineering.

He is currently working as a Graduate Teaching Assistant and researching in the Aerospace Systems Lab (ASL) with Dr. Kamesh Subbarao at the University of Texas at Arlington. His areas of interest include Unmanned Vehicle Systems, Unmanned Aerial Vehicles and Rotorcrafts.